



# **Conception et validation expérimentale de manoeuvres inspirées du réflexe de redressement du chat pour la réorientation d'un robot articulé en chute libre**

**Mémoire**

**Xavier Garant**

**Maîtrise en génie mécanique - avec mémoire**  
**Maître ès sciences (M. Sc.)**

Québec, Canada

**Conception et validation expérimentale de  
manœuvres inspirées du réflexe de redressement du  
chat pour la réorientation d'un robot articulé  
en chute libre**

**Mémoire**

**Xavier Garant**

Sous la direction de:

Clément Gosselin, directeur de recherche

# Résumé

Ce mémoire présente deux manœuvres permettant de modifier l'orientation d'un robot articulé en apesanteur, en n'utilisant que ses mouvements internes, à l'instar du réflexe de redressement du chat. Celles-ci ont comme caractéristique principale d'opérer ce changement malgré le fait qu'elles se traduisent par des boucles fermées dans l'espace articulaire du robot. Les manœuvres peuvent être exécutées séquentiellement, en variant leurs amplitudes, afin de rendre atteignable n'importe quelle orientation dans l'espace tridimensionnel. La dynamique des manœuvres est explorée en simulation afin d'identifier des paramètres favorables. Des exemples de réorientation sont présentés en simulation avec un modèle de robot à quatre membrures et trois articulations rototoïdes. Enfin, un prototype physique est construit à partir de ce modèle et les résultats numériques sont validés expérimentalement à l'aide d'une tour d'apesanteur et d'un système de capture de mouvements.

# Abstract

This Master's thesis introduces two distinct manoeuvres allowing a free-floating robot to reorient itself using its internal movements only, like the cat-righting reflex. The principal interest of these manoeuvres lies in the fact that they achieve this reorientation even though they are represented by closed loops in the joint space of the robot. The manoeuvres can be executed in sequence, with varying amplitude, in order to reach any orientation in three-dimensional space. Their dynamics are explored through numerical simulation in order to find favourable parameters. Reorientation examples are presented in simulation with a robot model composed of four links and three rotary actuators. Finally, a practical prototype is built from this model and the simulation results are experimentally validated using a drop tower and a motion capture system.

# Table des matières

Résumé	ii
Abstract	iii
Table des matières	iv
Liste des figures	vi
Remerciements	ix
Avant-propos	x
Introduction	1
<b>1 Design and Experimental Validation of a Manoeuvre Inspired from the Cat Righting Reflex for the Reorientation of a Free Falling Robot</b>	<b>4</b>
1.1 Résumé . . . . .	4
1.2 Abstract . . . . .	4
1.3 Introduction . . . . .	5
1.4 Reorientation Manoeuvre . . . . .	6
1.5 Mathematical Background . . . . .	7
1.6 Prototype Design . . . . .	10
1.7 Simulation . . . . .	11
1.8 Experimental Validation . . . . .	14
1.9 Conclusion . . . . .	15
1.10 Bibliographie . . . . .	18
<b>2 Reorientation of a free-floating robot using closed-loop paths in the joint space</b>	<b>20</b>
2.1 Résumé . . . . .	20
2.2 Abstract . . . . .	20
2.3 Introduction . . . . .	21
2.4 Rorrientation Manoeuvres . . . . .	22
2.5 Mathematical Background . . . . .	25
2.6 Prototype Design . . . . .	28
2.7 Simulation . . . . .	28
2.8 Experimental Validation . . . . .	33
2.9 Discussion . . . . .	35

2.10 Conclusion . . . . .	39
2.11 Bibliographie . . . . .	40
<b>3 Méthodologie</b>	<b>44</b>
3.1 Simulation numérique . . . . .	44
3.2 Validation expérimentale . . . . .	46
3.3 Conclusion . . . . .	53
3.4 Bibliographie . . . . .	53
<b>Conclusion</b>	<b>54</b>
<b>Bibliographie</b>	<b>56</b>

# Liste des figures

1.1	Manoeuvre steps for a six-body, five-joint architecture (left). Manoeuvre steps for a four-body, three-joint architecture (right) . . . . .	6
1.2	Geometric modelling of the robot . . . . .	9
1.3	CAD model of the prototype. Parts in blue are made of 3D-printed ABS plastic. Parts in grey are made of steel. . . . .	11
1.4	Dynamic simulation of the robot executing the manoeuvre. . . . .	11
1.5	Final orientation of the robot for different values of maximum joint displacement. . . . .	12
1.6	Final orientation of the robot for different values of moment of inertia of the end links. All simulations are for a maximum displacement of 270 degrees at the distal joints and 120 degrees at the central joint. . . . .	13
1.7	Final orientation of the robot for different values of rotor inertia and gearbox ratio. All simulations are for a maximum displacement of 270 degrees at the distal joints and 120 degrees at the central joint. . . . .	14
1.8	Still frames from the high speed footage . . . . .	16
1.9	Orientation of link 1 in space expressed with Euler angles $\alpha, \beta, \gamma$ following a ZXZ convention. Theoretical and measured joint coordinates for the manoeuvre. . . . .	17
2.1	Description of manoeuvre A : Manoeuvre steps for a six-body, five-joint architecture (left). Manoeuvre steps for a four-body, three-joint architecture (right). Thinner line stubs show link orientation. . . . .	23
2.2	Description of manoeuvre B : Front view, manoeuvre steps for a four-body, three-joint architecture (left). Side view, manoeuvre steps for a four-body, three-joint architecture (right). Thinner line stubs show link orientation. . . . .	24
2.3	Geometric modelling of the robot. . . . .	26
2.4	CAD model of the prototype. Parts in blue are made of 3D-printed ABS plastic. Parts in grey are made of steel. . . . .	28
2.5	Dynamic simulation of the robot executing manoeuvre A. . . . .	29
2.6	Dynamic simulation of the robot executing manoeuvre B. . . . .	29
2.7	Final orientation of the robot after manoeuvre A for different values of maximum joint displacement. . . . .	29
2.8	Final orientation of the robot after manoeuvre A for different values of moment of inertia of the end links. All simulations are for a maximum displacement of 270 degrees at the distal joints and 120 degrees at the central joint. . . . .	31
2.9	Final orientation of the robot after manoeuvre A for different values of rotor inertia and gearbox ratio. All simulations are for a maximum displacement of 270 degrees at the distal joints and 120 degrees at the central joint. . . . .	31

2.10	Final orientation of the robot after manoeuvre B for different values of maximum joint displacement. . . . .	32
2.11	Physical prototype with VICON reflective markers. . . . .	33
2.12	Still frames from the high speed footage of the robot executing manoeuvre A. .	34
2.13	Orientation of link 1 in space expressed with Euler angles $\alpha, \beta, \gamma$ following a ZXZ convention for manoeuvre A. Theoretical and measured joint coordinates for this manoeuvre. . . . .	36
2.14	Orientation of link 1 in space expressed with Euler angles $\alpha, \beta, \gamma$ following a ZXZ convention for manoeuvre B. Theoretical and measured joint coordinates for this manoeuvre. . . . .	37
2.15	Orientation of the robot at the end of each manoeuvre of the sequence. . . . .	38
3.1	Schéma du processus de simulation. . . . .	45
3.2	Courbes couple-vitesse pour l'articulation centrale, pour la première étape de la manoeuvre. Coin supérieur gauche : Durée de 110 ms, moteur sous-utilisé. Coin supérieur droit : Durée de 100 ms, moteur sous-utilisé. Coin inférieur gauche : Durée de 90 ms, moteur utilisé efficacement. Coin inférieur droit : Durée de 80 ms, moteur sur-utilisé. . . . .	46
3.3	Détail du montage expérimental. À gauche : Détail du système de déclenchement. À droite : Détail du panier servant à la réception du robot. . . . .	48
3.4	Diagramme de fonctionnement de la partie électronique du montage expérimental	48
3.5	Schéma de commande par couples pré-calculés. . . . .	49
3.6	Schéma du problème de changements de repère . . . . .	52

Comme des nains  
sur les épaules de géants

---

Bernard de Chartres

# Remerciements

Mes premiers remerciements vont à Clément Gosselin, qui en plus de m'avoir fait entrer dans le monde académique, m'y a aussi guidé par ses conseils éclairés. Merci de m'avoir donné ma chance il y a quelques années, de m'avoir fait confiance pendant mon cheminement et d'avoir toujours offert ton temps sans compter. J'ai adoré mon travail et cela t'est sans doute en grande partie attribuable.

Je tiens aussi à remercier Alexandre Campeau-Lecours et Philippe Cardou, qui m'ont également initié à la recherche. Votre passion pour votre vocation est contagieuse et ça a été un réel plaisir de vous côtoyer.

Je ne voudrais surtout pas passer sous silence la contribution de Thierry et Simon, deux véritables piliers du laboratoire. Toujours présents, autant dans l'ombre que sous les feux de la rampe, je vous assure que votre aide et votre apport ne passent pas inaperçus et je vous remercie mille fois pour ceux-ci.

À tous les membres du laboratoire que j'ai pu côtoyer, je dis merci pour les discussions enrichissantes, l'aide théorique ou technique que vous avez pu offrir, mais surtout pour les rires.

Finalement, je remercie mes parents, ma famille, mes amis et, bien entendu, ma partenaire de vie pour m'avoir offert un environnement sain et propice à l'épanouissement. Votre apport, bien que moins tangible, est aussi important que la somme de tous les autres.

# Avant-propos

Le présent ouvrage est écrit suivant la forme d'un mémoire par articles. Les deux premiers chapitres sont donc des articles scientifiques rédigés en cours d'études, dans le cadre de la recherche entreprise pour l'obtention du grade.

Le premier article a été soumis le 13 septembre 2018 à l'édition 2019 de l'*International Conference on Robotics and Automation* (ICRA). Cette conférence annuelle se déroule sous l'égide de l'*Institute of Electrical and Electronics Engineers* (IEEE). Vu le caractère international de la conférence, la langue de rédaction est l'anglais. Les travaux de recherche nécessaires à la préparation de cet article ont été réalisés par l'étudiant, sous la supervision du directeur de recherche et seul co-auteur Clément Gosselin. En ce sens, l'article a été rédigé par l'étudiant, puis revu par le directeur de recherche. L'étudiant est donc le premier auteur pour cette publication.

Le deuxième article est une version finale prête à la soumission à la revue scientifique *Transactions on Robotics* de l'IEEE. Le caractère international de la revue impose l'anglais comme langue de rédaction. La préparation de cet ouvrage a suivi un processus de publication que l'IEEE appelle évolutif, c'est-à-dire que l'article présente la suite des travaux soumis précédemment. Il reprend donc une partie du contenu de l'article précédent pour développer de nouvelles contributions, telles qu'énoncées ci-bas :

1. Une deuxième manoeuvre de réorientation est présentée. Cette manoeuvre permet au robot d'accomplir des rotations nettes autour d'un axe différent, tel que démontré en simulation.
2. Des essais expérimentaux supplémentaires établissent la validité de la simulation dynamique de cette deuxième manoeuvre.
3. Il est démontré que n'importe quelle orientation dans l'espace 3D peut être atteinte en ajoutant cette deuxième manoeuvre.
4. Une simulation dynamique supplémentaire appuie cette affirmation en montrant que le robot peut modifier son orientation de façon arbitraire en enchaînant les deux manoeuvres de façon alternée.

Ces nouvelles contributions sont le fruit de travaux de recherche réalisés par l'étudiant sous

la supervision du directeur. L'étudiant a donc rédigé l'article à titre de premier auteur, avec l'appui du directeur et seul co-auteur Clément Gosselin pour la révision.

Un chapitre additionnel expliquant la démarche expérimentale est inclus à la suite des deux articles. Cet ajout a été fait suivant les recommandations de la direction de programme, puisque le format compact des publications scientifiques tend à évacuer cette information. Ce chapitre est donc écrit dans l'optique de détailler les processus de simulation et de validation expérimentale qui ont mené aux conclusions finales.

# Introduction

Que ce soit en repoussant les frontières de l'inconnu par l'exploration spatiale, en reproduisant des gestes auparavant réservés au monde animal, ou en rivalisant avec la motricité de l'être humain, la robotique, telle que nous la connaissons aujourd'hui, a fait des bonds de géant depuis sa démocratisation au milieu du 20<sup>e</sup> siècle. En effet, bien que l'idée de sortir les robots du cadre manufacturier se soit imposée graduellement, elle est maintenant la source d'initiatives de recherche qui brouillent continuellement les limites du possible. En l'occurrence, un domaine de recherche découlant du décloisonnement des applications robotiques et qui établit un pont entre l'exploitation de l'espace et le biomimétisme est celui de la réorientation inertielle.

Kane et Scher (Kane and Scher, 1970) sont souvent cités à titre de précurseurs dans ce domaine, ayant établi un cadre mathématique permettant d'expliquer la réorientation du chat en chute libre. Le réflexe de redressement du chat, bien que d'apparence anodine, est néanmoins un exemple parfait d'un phénomène qui est resté une énigme pour la science jusqu'au milieu du siècle dernier. À juste titre, il paraît contre-intuitif qu'avec un moment cinétique nul et en l'absence de force externe, un simple corps articulé en chute libre puisse modifier son orientation dans l'espace. Pourtant, en y prêtant attention, on remarque que ce phénomène est présent partout autour de nous. D'autres animaux, tels que les lézards (Jusufi et al., 2010) tirent profit de cette stratégie. Sans elle, les plongeurs acrobatiques, gymnastes et trampolinistes amateurs comme professionnels seraient totalement démunis (Frohlich, 1980). Enfin, qui ne s'est jamais retrouvé à lever instinctivement les bras dans les airs pour se redresser au moment d'une chute sur la glace ?

Il s'avère que ce phénomène appartient à une classe de problèmes traitant des systèmes non holonomes. Conséquemment, l'état d'un tel système dépend de la trajectoire que suivent les paramètres qui le décrivent (Shapere, 1988). Cet état peut par ailleurs être modifié même si les paramètres du système reviennent à leur valeur initiale suivant une trajectoire fermée. Concrètement, ceci signifie qu'à l'instar d'un chat ou d'un trampoliniste, un robot peut se réorienter en suivant une séquence de mouvements qui ramène toutes ses articulations à leur position initiale.

Ce constat permet de dégager deux grands champs d'application où une telle capacité pourrait être bénéfique ou même essentielle. D'une part, un engin spatial équipé, par exemple, d'un

manipulateur robotique, pourrait modifier son orientation sans avoir recours à des propulseurs ou à des systèmes supplémentaires tels que des roues d'inertie. Dans un contexte où les débris et les satellites défectueux en orbite autour de la Terre posent un risque de plus en plus sérieux pour l'avenir de l'activité humaine dans l'espace, on peut s'attendre à ce que des satellites d'entretien, équipés de bras robotiques, deviennent une réalité dans un futur rapproché (Flores-Abad et al., 2014). D'autre part, la réorientation en chute libre peut s'avérer pratique pour les robots terrestres ayant la capacité de faire des sauts ou qui sont potentiellement sujets à des chutes. Dans ce contexte, la possibilité de modifier l'orientation du robot, de manière à amoindrir le potentiel de dommage causé par un impact avec le sol devient en effet très intéressante.

## Objectifs du mémoire

L'objectif des travaux de recherche présentés dans ce mémoire est donc d'étudier la problématique de la réorientation des robots articulés en chute libre, soumis à un moment cinétique nul. Plus précisément, les objectifs sont de :

1. Développer une stratégie de réorientation réalisable dans l'espace tridimensionnel, permettant d'atteindre une orientation finale arbitraire.
2. Simuler le comportement dynamique du robot avec l'aide d'outils numériques afin de valider la stratégie proposée.
3. Concevoir un montage physique et une méthode permettant la validation expérimentale des résultats obtenus en simulation.

## Structure du mémoire

Le premier chapitre de ce mémoire présente l'étude d'une première manœuvre de réorientation analogue au réflexe de redressement du chat. L'effet de l'amplitude des mouvements articulaires sur le comportement de la manœuvre, ainsi que l'impact de paramètres de conception importants sont explorés à l'aide de simulations dynamiques. Enfin, les résultats des simulations sont validés expérimentalement.

Le second chapitre reprend une partie du contenu du premier chapitre pour présenter une deuxième manœuvre de réorientation. Cette dernière est réalisable par le même robot sans nécessiter de modifications. Le comportement dynamique de cette deuxième manœuvre est également étudié en simulation. Ensuite, une validation expérimentale appuie les résultats obtenus et permet de comparer les deux manœuvres. Enfin, dans la dernière section du chapitre est discutée la possibilité d'atteindre une orientation arbitraire en utilisant seulement ces deux manœuvres.

## Bibliographie

- A. Flores-Abad, O. Ma, K. Pham, and S. Ulrich. A review of space robotics technologies for on-orbit servicing. *Progress in Aerospace Sciences*, 68 :1–26, jul 2014.
- C. Frohlich. The Physics of Somersaulting and Twisting. *Scientific American*, 242 :154–165, 1980.
- A. Jusufi, D. T. Kawano, T. Libby, and R. J. Full. Righting and turning in mid-air using appendage inertia : Reptile tails, analytical models and bio-inspired robots. *Bioinspir. Biomim.* 5 045001 *Bioinsp. Biomim.*, 5 :45001–12, 2010.
- T. Kane and M. Scher. Human self-rotation by means of limb movements. *Journal of Biomechanics*, 3(1) :39–49, jan 1970.
- A. D. Shapere. *Gauge mechanics of deformable bodies*. PhD thesis, University of California, Santa Barbara, 1988.

# Chapitre 1

## Design and Experimental Validation of a Manoeuvre Inspired from the Cat Righting Reflex for the Reorientation of a Free Falling Robot

### 1.1 Résumé

Cet article présente une manœuvre permettant à un robot d'exécuter des rotations selon son axe longitudinal par le biais de trajectoires fermées dans l'espace articulaire. Il est montré par simulation dynamique que l'amplitude de la rotation nette dépend de l'amplitude du déplacement angulaire des articulations. Avec des limites articulaires réalistes, le robot, qui ne possède que des articulations rototoïdes, est en mesure d'exécuter une rotation de 180 degrés similaire au réflexe de redressement du chat. Les résultats obtenus en simulation sont validés expérimentalement avec un prototype et un système de capture de mouvements VICON.

### 1.2 Abstract

This paper presents a manoeuvre allowing an articulated robot in free fall to rotate along its longitudinal axis using closed-loop paths in the joint space. It is shown through dynamics simulations that the magnitude of the net rotation is dependent upon the amplitude of angular displacement. With realistic joint limitations, the robot, which incorporates rotary actuators only, can perform a 180-degree reorientation similar to the cat righting reflex. The simulation results are experimentally validated with a prototype and a VICON motion tracking system.

### 1.3 Introduction

The elusive phenomenon of the self-righting cat falls under the category of problems governed by the law of constant angular momentum. Indeed, with nothing to push against, the cat manages to modify its orientation while free falling, by using the movements of its spine and limbs exclusively. Kane and Scher (Kane and Scher, 1969) were among the firsts to prove that a simplified mathematical model-cat could accomplish a 180 degree flip by executing a specific sequence of movements of the spine. Naturally, several research initiatives in the field of robotics sprouted from the study of this particular phenomenon, and the more general case of reorienting a mechanical system of articulated bodies (Shapere and Wilczek, 1989). As a matter of fact, it is nowadays possible to consider applications where having this ability is not only relevant but essential for a robot. Notably, posture control while falling to mitigate impact for articulated robots was investigated in (Yang et al., 2011; Bingham et al., 2014). Lizard-like self-righting through the use of a tail was studied with simplified systems composed of two bodies in (Jusufi et al., 2010; Chang-Siu et al., 2011; Zhao et al., 2015). However, most of the theoretical research in this area is centred on space systems and satellite control. The ability to control the orientation of multi-body space systems using internal movements could notably reduce the amount of propellant needed and save weight by removing the need for auxiliary systems such as reaction wheels or magnetic torquers. Several modelling methods have been proposed for free-floating space manipulators, like the virtual manipulator approach (Dubowsky and Papadopoulos, 1993) and the generalized Jacobian (Yoshida and Umetani, 1993). Nonlinear control models based on Lie brackets and controllability for this case of nonholonomic problem have also been investigated in depth (Reyhanoglu and McClamroch, 1992; Kolmanovsky et al., 1995; Rui et al., 1997, 2000).

This article proposes a manoeuvre for reorienting an articulated robot under zero angular momentum in a weightless environment. Much like the cat motion itself, the method relies on closed paths (loops) in the joint space to produce a net change in orientation. With reasonable joint limits, the manoeuvre allows for a 180 degree net rotation about the longitudinal axis of the robot. The manoeuvre can also be repeated any number of times with different movement amplitudes to achieve a desired rotation.

While much theoretical work has been done on orienting multi-body systems in free fall, to the best of the knowledge of the authors, few research papers provide experimental validation of the results in 3D space. This may be due in part to the challenge that reproducing weightlessness conditions represents. In a previous paper, a planar mechanism was proposed (Bettez-Bouchard and Gosselin, 2016) for validation purposes. However, due to the planar architecture of the robot, the manoeuvres required the robot to collide with itself. In practice, manipulators have joint limits to prevent self-collision. One example of an experimentally validated robot capable of righting itself in free fall while incorporating joint limitations is presented in (Mather and Yim, 2009). However, the method that is used requires that an actuated Hooke joint be

positioned centrally on the robot, which limits its practicality. The present paper aims at addressing the above considerations.

This paper is structured as follows. The proposed reorientation manoeuvre is first described in Section 1.4. Then, the mathematical model, which is based on the conservation of angular momentum, is introduced in Section 1.5. Section 1.6 presents the design of the prototype of an articulated robot on which the proposed manoeuvre is implemented. Simulation results obtained with a dynamic simulation program are then presented in Section 1.7, where the effects of some of the design parameters on the reorientation are studied and discussed. Section 1.8 presents the experimental validation of the manoeuvre using the physical 3-dof articulated prototype. Finally, conclusions are drawn in Section 1.9.

## 1.4 Reorientation Manoeuvre

The proposed manoeuvre can be decomposed in six steps, as shown in Figure 1.1. Transposing this method to the falling cat would imply that the animal twists its body along the spine axis, as opposed to Kane and Scher's "no-twist" model. There are diverging opinions on whether the cat effectively does so (Frohlich, 1979). However, the manoeuvre is comparable to a "swivel-hips" that trampolinists execute to rotate their body 180 degrees (Frohlich, 1979).

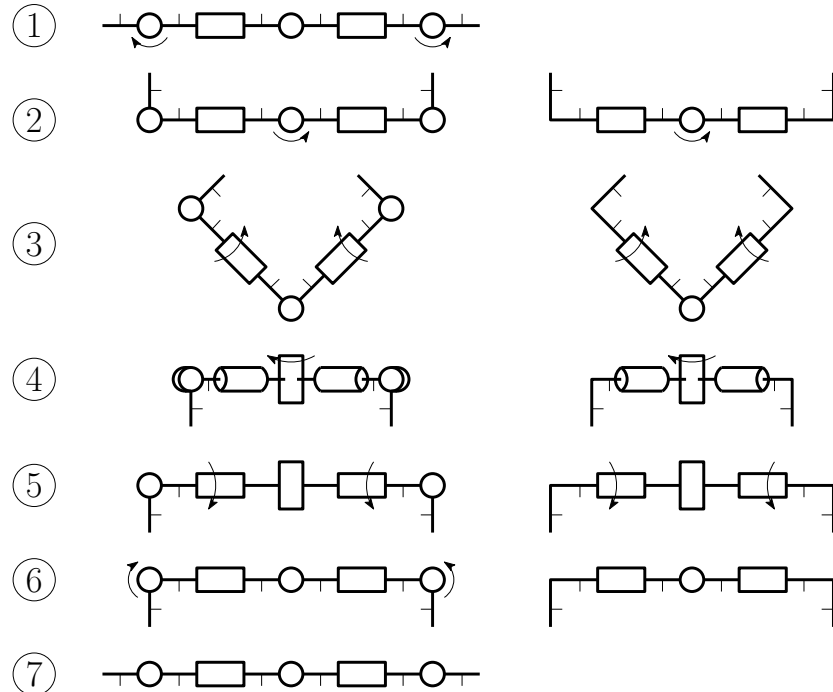


FIGURE 1.1 – Manoeuvre steps for a six-body, five-joint architecture (left). Manoeuvre steps for a four-body, three-joint architecture (right).

The manoeuvre is well suited for a serial articulated robot composed of six bodies and five

rotary actuators. However, the system can be reduced to four bodies and three rotary actuators for simplicity, without notable loss of performance. We can discard steps 1 and 6 and use an "L" shape for the first and last links of the chain, without actuators 1 and 5, as shown in Figure 1.1. This simplifies the experimental process by reducing the number of control inputs and allowing more time for the most important parts of the sequence before the robot touches the ground.

The manoeuvre works by changing the moment of inertia of certain parts of the system between each actuation of the joints. For instance, at step 3, when actuating joint 2 of the six-body system, the moment of inertia (with respect to the joint axis) of the combined bodies to the right of the joint is much larger than the moment of inertia of the bodies to the left. Thus, qualitatively, the left segment will be subject to a large rotation, while the right segment will experience little rotation. By contrast, at step 5, the relative moments of inertia of the left and right sides are similar, therefore both sides will rotate by a similar amount. This way, the relative angle between each link always returns to its original value at the end of the manoeuvre, effectively meaning that the robot goes back to its starting configuration in the joint space.

This type of manoeuvre, when executed in free-fall, has the interesting characteristic of being time-independent. In other words, the speed at which the manoeuvre is executed has no impact on the final state of the system : only the geometric path matters. A mathematical proof of this property can be found in (Shapere, 1988). Thus, we can use a representation of the trajectories in joint space without losing significant information, and use this to our advantage for easier parametrization of the trajectories. The proposed manoeuvre for the simplified three-joint architecture is then represented as a closed path in the joint-space.

## 1.5 Mathematical Background

In order to provide a better understanding of the physics at play during the reorientation, the dynamic model of a free floating serial robot with  $n$  links and  $j$  revolute joints ( $j = n - 1$ ) is derived in this section. The formulation presented here was proposed in (Bettez-Bouchard and Gosselin, 2016) as an adaptation of (Dubowsky and Papadopoulos, 1993).

Free floating manipulators differ from their earth-based counterparts in that the position and orientation of each link depend on the position and orientation of every other link in the chain (Wittenburg, 2007). As a consequence of the conservation of momentum, the dynamic behaviour of a free floating multibody system can be expressed with respect to its global centre of mass ( $CM$ ), as shown in Figure 1.2. Since the position of the  $CM$  is constant in a reference frame  $R_0$  moving with the robot, the position  $\mathbf{r}_i$  and velocity  $\mathbf{v}_i$  of the centre of mass ( $CM_i$ ) of link  $i$  ( $i = 1, \dots, n$ ) is related to that of the other bodies as follows

$$\sum_{i=1}^n m_i \mathbf{r}_i = \mathbf{0} \quad (1.1)$$

and

$$\sum_{i=1}^n m_i \mathbf{v}_i = \mathbf{0} \quad (1.2)$$

where  $m_i$  is the mass of link  $i$ . Moreover, the conservation of the angular momentum leads to

$$\frac{d\mathbf{h}}{dt} = \mathbf{0} \quad (1.3)$$

with

$$\mathbf{h} = \sum_{i=1}^n (\mathbf{I}_i \boldsymbol{\omega}_i + m_i \mathbf{r}_i \times \mathbf{v}_i) \quad (1.4)$$

where  $\mathbf{h}$  is the angular momentum,  $\mathbf{I}_i$  is the inertia tensor of link  $i$  and  $\boldsymbol{\omega}_i$  is its angular velocity. As previously stated, it is assumed that the robot is initially at rest ( $\boldsymbol{\omega}_i = \mathbf{v}_i = \mathbf{0}, i = 1, \dots, n$ ) and that no external torque is applied to it during the reorientation, thus  $\mathbf{h}$  is set to  $\mathbf{0}$ .

To compute (1.4), each term must be expressed in the same reference frame, in this case  $R_0$ . The rotation from reference frame  $i - 1$  to reference frame  $i$  can be expressed with matrix  $\mathbf{Q}_i$  using an axis angle representation. With  $\theta_i$  the rotation angle about unit vector  $\underline{\mathbf{e}}_i$  (expressed in its local reference frame) corresponding to the axis of the  $i$ th revolute joint, this yields

$$\mathbf{Q}_i = \underline{\mathbf{e}}_{i-1} \underline{\mathbf{e}}_{i-1}^T + c_i (\mathbf{1} - \underline{\mathbf{e}}_{i-1} \underline{\mathbf{e}}_{i-1}^T) + s_i \mathbf{1} \times \underline{\mathbf{e}}_{i-1} \quad i = 2, \dots, n \quad (1.5)$$

with

$$\mathbf{1} \times \mathbf{e}_i = \begin{bmatrix} 0 & -e_{i3} & e_{i2} \\ e_{i3} & 0 & -e_{i1} \\ -e_{i2} & e_{i1} & 0 \end{bmatrix} \quad (1.6)$$

and where  $c_i$  and  $s_i$  respectively stand for  $\cos \theta_i$  and  $\sin \theta_i$ , while  $\mathbf{1}$  stands for the  $3 \times 3$  identity matrix. Matrix  $\mathbf{Q}_1$  corresponds to the rotation from the inertial reference frame to link 1. The representation in  $R_0$  is then obtained by pre-multiplying by the product of rotation matrices  $\mathbf{Q}_1$  to  $\mathbf{Q}_i$  in the case of a vector, and also by post-multiplying by the transpose of these rotation matrices in the case of a tensor. For instance,  $\mathbf{e}_i$  and  $\mathbf{I}_i$ , which are expressed in  $R_0$ , are obtained as

$$\mathbf{e}_i = \left( \prod_1^i \mathbf{Q}_i \right) \underline{\mathbf{e}}_i \quad (1.7)$$

$$\mathbf{I}_i = \left( \prod_1^i \mathbf{Q}_i \right) \underline{\mathbf{I}}_i \left( \prod_1^i \mathbf{Q}_i^T \right) \quad (1.8)$$

where an underscore implies that the vector or tensor is expressed in its local reference frame.

Next,  $\mathbf{r}_i$ ,  $\mathbf{v}_i$  and  $\boldsymbol{\omega}_i$  must be explicated. The derivation of these terms is based on the concept of barycentre (Wittenburg, 2007), adapted to free floating serial manipulators in (Bettez-Bouchard and Gosselin, 2016; Dubowsky and Papadopoulos, 1993). For each link, two constant

construction vectors are defined, namely  $\underline{\mathbf{r}}_{0i}$  and  $\mathbf{l}_{0i}$ , as shown in Figure 1.2. Vector  $\underline{\mathbf{r}}_{0i}$  connects  $CM_i$  to joint  $i$ , while vector  $\mathbf{l}_{0i}$  connects  $CM_i$  to joint  $i - 1$ .

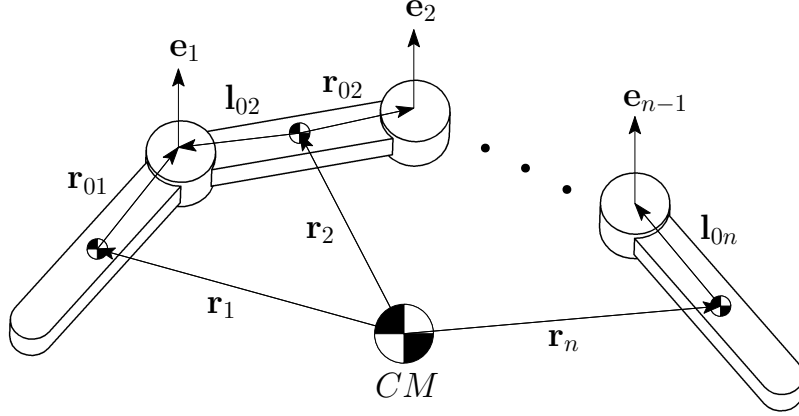


FIGURE 1.2 – Geometric modelling of the robot.

Combining these vectors with the mass of the links yields the position of the barycentre  $\mathbf{c}_{0i}$ , which is given by

$$\mathbf{c}_{0i} = \mathbf{l}_{0i}\mu_i + \mathbf{r}_{0i}(1 - \mu_{i+1}) \quad (1.9)$$

with  $\mu_i$  the mass distribution in the robot, given by

$$\mu_i = \begin{cases} 0 & i = 1 \\ \sum_{k=1}^{i-1} \frac{m_k}{M} & i = 2, \dots, n \\ 1 & i = n + 1 \end{cases} \quad (1.10)$$

where  $M$  is the total mass of the robot. Vector  $\mathbf{c}_{0i}$  can equivalently be found by adding a point mass  $M\mu_i$  to joint  $i - 1$  and  $M(1 - \mu_{i+1})$  to joint  $i$ , which defines an augmented link (Wittenburg, 2007). The barycentre then becomes the centre of mass of this augmented link (Dubowsky and Papadopoulos, 1993). New augmented construction vectors can be defined with respect to this centre of mass, as

$$\underline{\mathbf{c}}_{0i}^* = -\underline{\mathbf{c}}_{0i} \quad (1.11)$$

$$\underline{\mathbf{r}}_{0i}^* = \underline{\mathbf{r}}_{0i} - \underline{\mathbf{c}}_{0i} \quad (1.12)$$

$$\mathbf{l}_{0i}^* = \mathbf{l}_{0i} - \underline{\mathbf{c}}_{0i} \quad (1.13)$$

Similarly to vector  $\mathbf{r}_i$ , these vectors are fully specified by the configuration of the robot, which depends on the joint angles collected in vector  $\boldsymbol{\theta}$ . It can be shown that  $\mathbf{r}_i$  can be expressed in terms of the barycentric vectors, which yields

$$\mathbf{r}_i = \sum_{k=1}^n \mathbf{b}_{ki} \quad (1.14)$$

with  $\mathbf{b}_{ki}$  defined using the following rule

$$\mathbf{b}_{ki} = \begin{cases} \mathbf{l}_{0k}^* & k > i \\ \mathbf{c}_{0k}^* & k = i \\ \mathbf{r}_{0k}^* & k < i \end{cases}. \quad (1.15)$$

Vector  $\boldsymbol{\omega}_i$  can be expressed in  $R_0$  by adding the angular velocity vector imparted by each joint with the angular velocity  $\boldsymbol{\omega}_1$  of the first link, which yields

$$\boldsymbol{\omega}_i = \begin{cases} \boldsymbol{\omega}_1 & i = 1 \\ \boldsymbol{\omega}_{i-1} + \mathbf{e}_{i-1}\dot{\theta}_{i-1} & i = 2, \dots, n. \end{cases} \quad (1.16)$$

Considering that vector  $\mathbf{b}_{ki}$  is constant in the reference frame moving with angular velocity  $\boldsymbol{\omega}_i$ ,  $\mathbf{v}_i$  is obtained as

$$\mathbf{v}_i = \sum_{k=1}^n \boldsymbol{\omega}_k \times \mathbf{b}_{ki} \quad i = 1, \dots, n. \quad (1.17)$$

Equation (1.17) can be rearranged with the help of (1.16), yielding

$$\mathbf{v}_i = \boldsymbol{\omega}_1 \times \mathbf{r}_i + \mathbf{C}_i \dot{\boldsymbol{\theta}} \quad (1.18)$$

where  $\mathbf{C}_i$  is a matrix of dimension  $3 \times j$  which is a function of the construction parameters of the robot.

Equations (1.14), (1.16) and (1.18) can now be substituted into (1.4) — where  $\mathbf{h}$  is set to zero — to form a system of equations that depends only on the unknowns  $\boldsymbol{\omega}_1$  and  $\dot{\boldsymbol{\theta}}$ . The double vector product obtained in the process can be rearranged as

$$m_i \mathbf{r}_i \times (\boldsymbol{\omega}_1 \times \mathbf{r}_i) = m_i ((\mathbf{r}_i^T \mathbf{r}_i) \mathbf{1} - \mathbf{r}_i \mathbf{r}_i^T) \boldsymbol{\omega}_1. \quad (1.19)$$

Finally, collecting the terms in  $\boldsymbol{\omega}_1$  on one side and the terms in  $\dot{\boldsymbol{\theta}}$  on the other side, a linear system of equations that relates the angular velocity of the first body and the joint velocity vector of the robot is obtained as

$$\mathbf{A} \boldsymbol{\omega}_1 = \mathbf{B} \dot{\boldsymbol{\theta}} \quad (1.20)$$

where  $\mathbf{A}$  is a  $3 \times 3$  matrix and  $\mathbf{B}$  is a matrix of dimension  $3 \times j$ , which both depend on the mass of the links, the geometric parameters and the configuration of the robot. This formulation of the dynamic model is general and is applicable to any spatial or planar serial free-floating robot.

## 1.6 Prototype Design

Based on the simplified three-joint architecture presented in Section 1.4, an experimental prototype was designed and built. A CAD model of the prototype is shown in Fig 1.3. The

robot was designed without any on-board electronics except for the motors themselves. One drawback of this design is that it requires an experimental setup where cables must run between each motor and an external controller for power and encoder signals. The measures that were taken to mitigate the influence of the hanging cables are addressed in more details in Section 1.8.

The total mass of the robot is approximately 0.3 kg. Machined steel inserts were added to the ends of links 1 and 4 in order to position their centre of mass in a way that favours the reorientation. Links 2 and 3 are hollow, allowing motors to be mounted inside them. The motors are 4.5 Watt brushed DC *RE-max 17* with 24:1 gearheads and 512 counts per turn encoders.

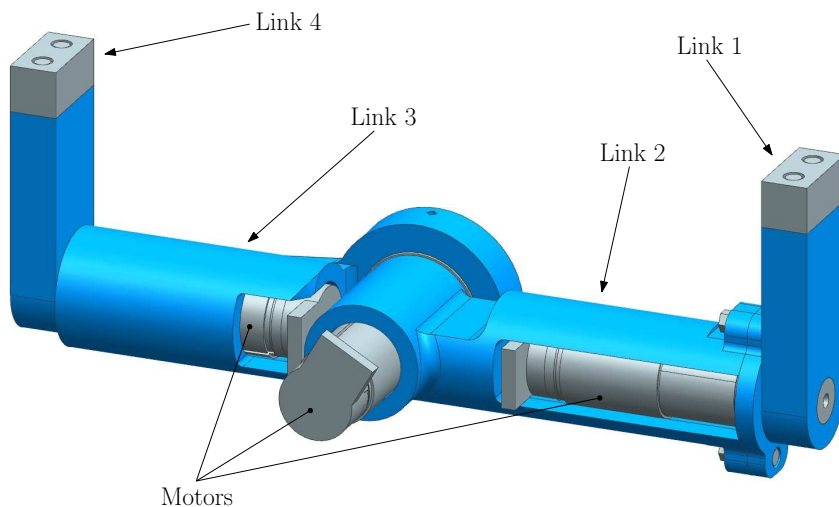


FIGURE 1.3 – CAD model of the prototype. Parts in blue are made of 3D-printed ABS plastic. Parts in grey are made of steel.

## 1.7 Simulation

Using the CAD model, dynamic simulations were performed using Siemens NX to study the effects of various parameters on the dynamics of the robot in zero-gravity. Figure 1.4 shows the progression of the reorientation manoeuvre simulated with the CAD model.



FIGURE 1.4 – Dynamic simulation of the robot executing the manoeuvre.

### 1.7.1 Trajectory in the joint space

The influence of the amplitudes of the movements on the net change in orientation was first investigated. In the joint space, this is equivalent to varying the dimensions of the rectangle loop that represents the trajectory. The final orientation as a function of maximum joint displacement is presented in Figure 1.5.

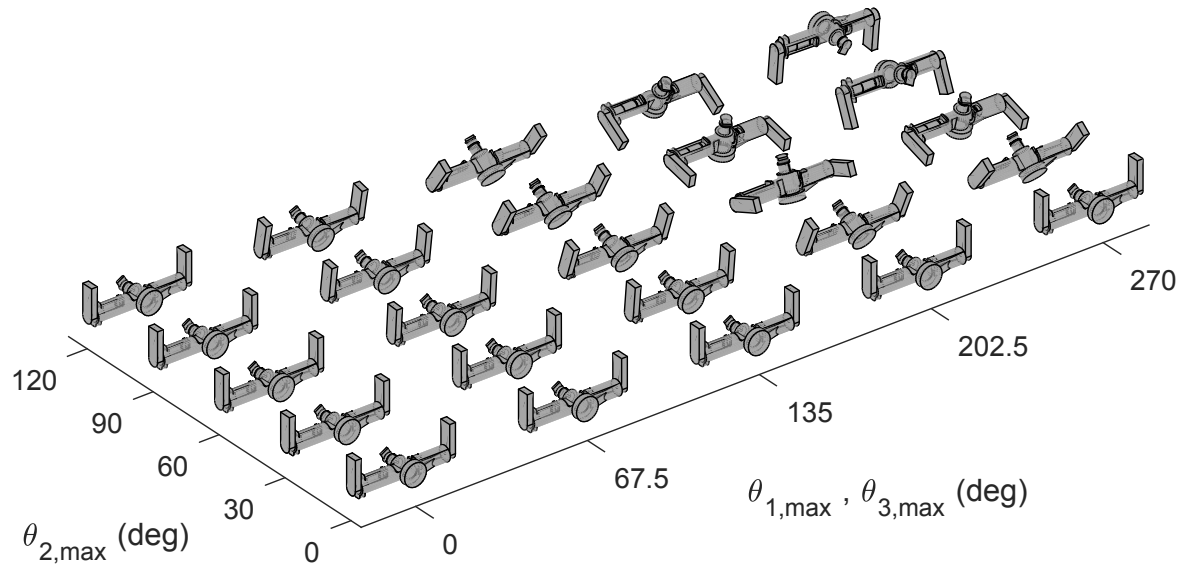


FIGURE 1.5 – Final orientation of the robot for different values of maximum joint displacement.

As it can be observed, the axis describing the net rotation induced by the manoeuvre varies very little with respect to maximum joint displacement. This means that the manoeuvre produces a rotation almost purely about the roll axis of the robot and that undesirable motions around other axes are almost nonexistent. In addition, the net rotation itself increases smoothly with respect to the maximum movement amplitude of both joints. Therefore, small internal movements of the robot produce a small reorientation while large internal movements produce a large reorientation, meaning that the manoeuvre behaves predictably. Moreover, with a reasonable displacement limit of 270 degrees for the distal joints and 120 degrees for the centre joint, a net rotation of approximately 180 degrees is predicted by the simulation. For a cat-like reorientation, a half-turn is the worst case scenario, since a rotation of more than 180 degrees is equivalent to a smaller rotation in the opposite direction. Practically, rotating in the opposite direction can be done by reversing the direction of rotation of joints 1 and 3.

### 1.7.2 Moment of inertia of the end links

The effect of different inertial parameters on the manoeuvre was also studied. The starting point of this analysis is the realization that drastically increasing the moments of inertia of

links 2 and 3 results in no reorientation. Indeed, having bodies 1 and 4 linked to a very high inertia would be comparable to fixing the stators of motors 1 and 3 in space. For this reason, the study was focused on the moment of inertia of links 1 and 4 about joint axes 1 and 3, respectively. Figure 1.6 shows the resulting net rotation for different values of moment of inertia, with the same prescribed joint trajectories for each simulation. For this robot, it can be observed that a moment of inertia of up to approximately 100 kg-mm<sup>2</sup> contributes to the desired reorientation, that is, a net rotation of 180 degrees. Increasing the inertia past this point has adverse effects on the manoeuvre, notably inducing a progressively greater amount of off-axis rotation and reducing the net amount of rotation about the principal axis of the robot. Moreover, a greater moment of inertia would require higher torques at joints 1 and 3 in order to accomplish the manoeuvre.

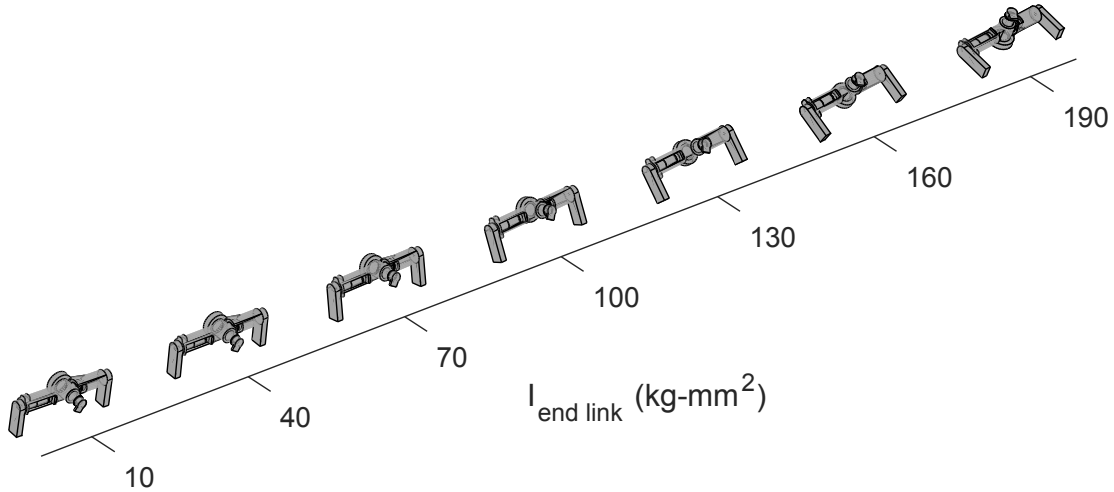


FIGURE 1.6 – Final orientation of the robot for different values of moment of inertia of the end links. All simulations are for a maximum displacement of 270 degrees at the distal joints and 120 degrees at the central joint.

### 1.7.3 Motor gear ratio and rotor inertia

With weightless robots, extra care must be taken in the selection of the motors for joint actuation. Indeed, the motors can significantly influence the dynamic behaviour of the robot in free fall, depending on their properties. For instance, a servomotor with a very high reduction ratio might offer more torque, but its fast spinning rotor may disturb the manoeuvre. To better characterize the influence of the gear ratio and the rotor inertia on the manoeuvre, simulations were performed with different values of these parameters. The results are shown in Figure 1.7.

It can be observed that for this specific manoeuvre and geometric configuration, increasing

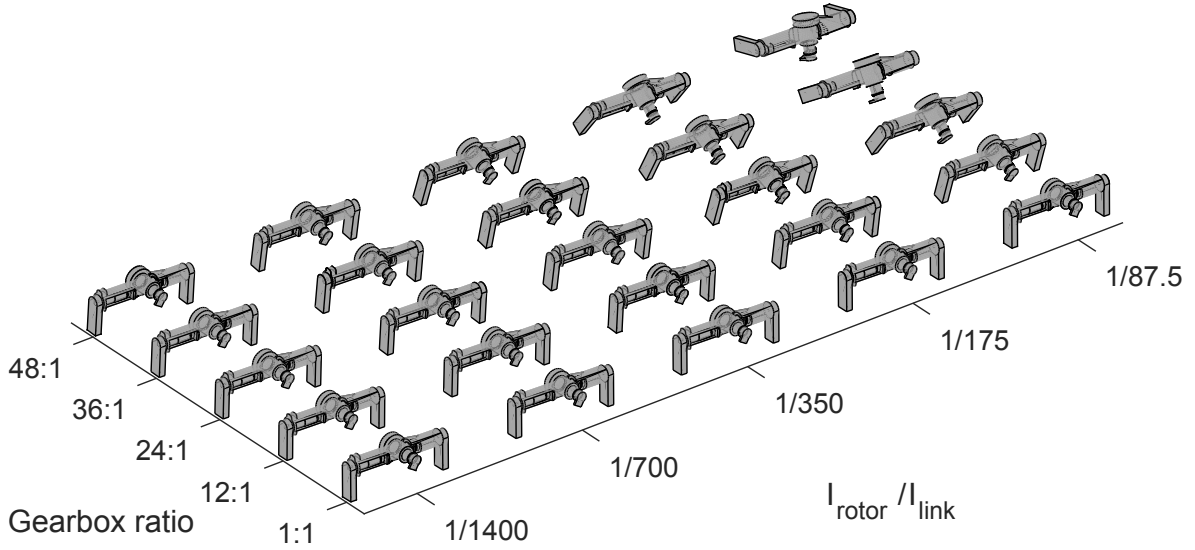


FIGURE 1.7 – Final orientation of the robot for different values of rotor inertia and gearbox ratio. All simulations are for a maximum displacement of 270 degrees at the distal joints and 120 degrees at the central joint.

both the moment of inertia of the rotor and the reduction ratio results in a greater net reorientation. In other words, a smaller maximum displacement at the joints would be sufficient to achieve a net rotation of 180 degrees about the roll axis of the robot. Still, there is a trade-off between performance, form factor, weight and availability of parts, which explains the choice of a 24:1 ratio and rotor inertia of  $0.1 \text{ kg-mm}^2$  for the current robot.

## 1.8 Experimental Validation

In order to validate the simulation results, the robotic prototype presented in Section 1.6 was built and an experimental set-up was designed. The drop post shown in the background in Figure 1.8 allows 2 metres of free fall, which is equivalent to approximately 0.6 second of weightlessness. The robot lands in a flexible basket mounted on a damped spring at the end of the drop. In order to limit the influence of initial conditions as much as possible, the release mechanism is a set of two electromagnets. The robot is completely still before release and the manoeuvre only begins 0.02 second after the electrical signal is sent to the electromagnets, to ensure that the robot is effectively released and to prevent any contact with the magnets during the manoeuvre. As mentioned in Section 1.6, the robot has no on-board electronics. To mitigate the influence of the cables connecting the robot to the controller, the thinnest possible extra flexible silicon insulated wires were used. In addition, a third electromagnet releases the wires simultaneously with the robot. This prevents the wires from pulling on the robot at the

instant of release and inducing angular momentum. When the fall is initiated, both the robot and the wires are weightless, thus the manoeuvre is only affected by the relatively small inertia of the wires.

For practical reasons, the drop height is limited. Thus, it is necessary to verify that the motors have enough power to execute the manoeuvre in the allowed time. To this end, the torque and speed values at each time step are extracted from the dynamic simulations of the manoeuvre and compared against the torque-speed limiting curve of the motors provided by the manufacturer. The allotted time for each step of the manoeuvre is then iteratively adjusted until a minimum-time trajectory is obtained.

It is important to note that the only control input to this robot is the relative angle between each pair of consecutive links. This means that while joints 1, 2 and 3 follow a prescribed trajectory through the use of a PID position control, the orientation of the robot in 3D space is only observed.

For qualitative analysis, the robot was filmed with a high speed camera at 800 frames per second. Figure 1.8 presents still frames from a typical test drop. From these images, it can be observed that the orientation of the robot follows what was predicted by the simulations. The prototype accomplishes a half-turn net rotation at the end of the prescribed sequence of joint movements, even with the wires linked to a fixed controller.

For quantitative validation of the observations, the orientation of the first link of the robot was tracked using a VICON motion capture system at a sampling rate of 300 Hz. The markers that are required for tracking have a negligible mass and were positioned on the body so as not to hinder the manoeuvre. Figure 1.9 shows the progression of the orientation with a ZXZ Euler angle representation. It can be clearly observed that the second and third angles return to their initial value at the end of the fall, while the first angle increases by 3.35 rad. With this convention, the first angle corresponds to the roll axis of the robot. This rotation of just over 180 degrees is what was predicted by the simulation. Figure 1.9 also shows that while joint coordinates did not exactly follow the prescribed curves,  $\theta_1$  and  $\theta_3$  stayed synchronised and each articulation reached the desired angular value at the prescribed time without any overlap between  $\theta_2$  and  $\theta_1$  or  $\theta_3$ . Thus, the data show that the reorientation can be considered successful. Moreover, the experimentally measured orientation of link 1 closely follows the simulation results, with a RMS error of 0.24 rad ( $13.8^\circ$ ) on the first angle, 0.21 rad ( $12^\circ$ ) on the second angle and 0.14 rad ( $8^\circ$ ) on the third angle.

## 1.9 Conclusion

A reorientation manoeuvre was elaborated and tested with a robotic prototype. The cat-like movement sequence achieved a net rotation of a half-turn almost purely about the longitudinal

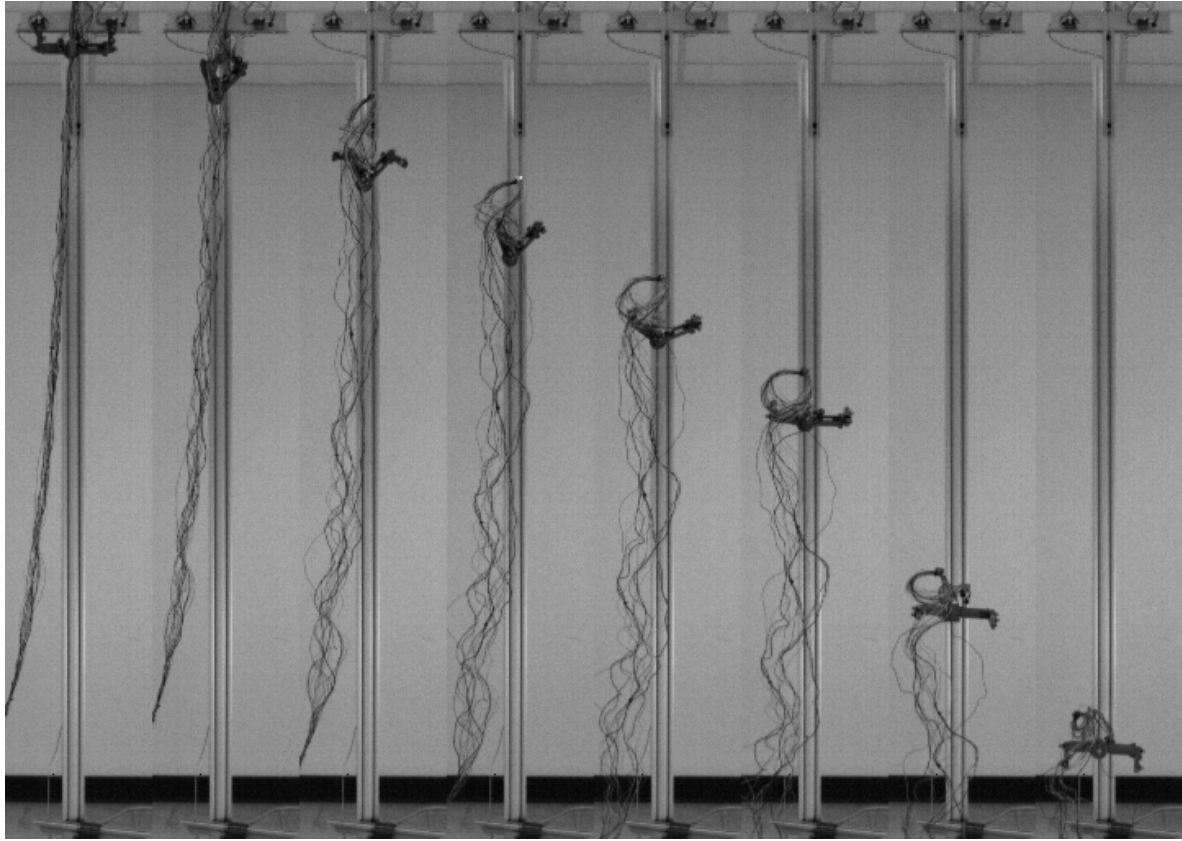


FIGURE 1.8 – Still frames from the high speed footage

axis of the robot. Furthermore, the manoeuvre proved stable with respect to maximum joint displacement. That is, lowering the limits on either the central or distal joints only resulted in a smaller net rotation about the same axis. Thus, a large rotation about a single axis can be decomposed as a repetition of smaller rotations : the same manoeuvre can be repeated any number of times to achieve an arbitrary rotation about a single axis. Admittedly, this may be impossible for terrestrial robots in free fall, since time is limited by the height of the fall. However, space robots benefit from having a virtually infinite amount of time to accomplish a sequence of manoeuvres. In that case, the movements can be made arbitrarily slow and the joint limits decreased to reduce the required torques at the joints and improve the safety margin for self-collision.

It is also worth restating that the presented proof of concept prototype was specifically designed with the intent of validating the proposed manoeuvre. Still, the manoeuvre lends itself to a typical 7-DoF shoulder-elbow-wrist serial manipulator architecture. This type of serial robot is frequent in space applications and notable examples include Canadarm2, the European Robotic Arm and the DARPA FREND arm (Flores-Abad et al., 2014).

A limitation of our study is that the proposed manoeuvres only work as intended in the absence

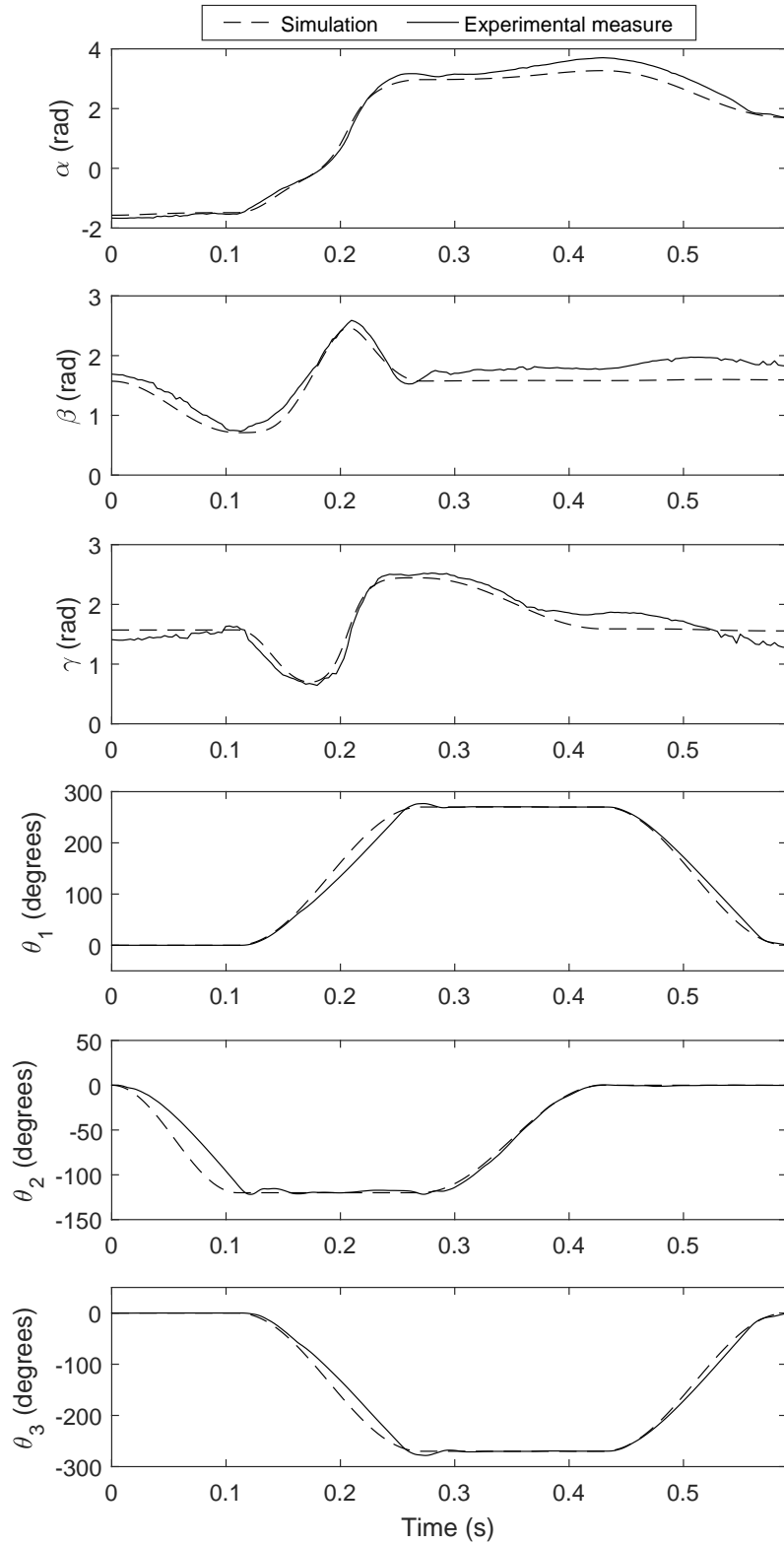


FIGURE 1.9 – Orientation of link 1 in space expressed with Euler angles  $\alpha, \beta, \gamma$  following a ZXZ convention. Theoretical and measured joint coordinates for the manoeuvre.

of angular momentum. If the robot already has angular momentum, moving its links can result in off-axis spins that are more complex to predict, such as when a diver performs a twisting somersault (Frohlich, 1979). Another limitation is the fact that while the motors in the joints of the robot are controlled in closed-loop, its orientation in 3D space is only controlled in open-loop. As previously stated, there are no on-board electronics, hence no sensors for feedback and reaction to disturbances. Consequently, future work will consist in developing a control method to dynamically adapt the basic joint trajectories for improved accuracy and stability on the orientation of the robot.

## 1.10 Bibliographie

- J.-A. Bettez-Bouchard and C. Gosselin. Development and experimental validation of a re-orientation algorithm for a free-floating serial manipulator. In *2016 IEEE International Conference on Robotics and Automation (ICRA)*, pages 2733–2738. IEEE, may 2016.
- J. T. Bingham, J. Lee, R. N. Haksar, J. Ueda, and C. K. Liu. Orienting in mid-air through configuration changes to achieve a rolling landing for reducing impact after a fall. In *2014 IEEE/RSJ International Conference on Intelligent Robots and Systems*, pages 3610–3617. IEEE, sep 2014.
- E. Chang-Siu, T. Libby, M. Tomizuka, and R. J. Full. A lizard-inspired active tail enables rapid maneuvers and dynamic stabilization in a terrestrial robot. In *2011 IEEE/RSJ International Conference on Intelligent Robots and Systems*, pages 1887–1894. IEEE, sep 2011.
- S. Dubowsky and E. Papadopoulos. The kinematics, dynamics, and control of free-flying and free-floating space robotic systems. *IEEE Transactions on Robotics and Automation*, 9(5) : 531–543, 1993.
- A. Flores-Abad, O. Ma, K. Pham, and S. Ulrich. A review of space robotics technologies for on-orbit servicing. *Progress in Aerospace Sciences*, 68 :1–26, jul 2014.
- C. Frohlich. Do springboard divers violate angular momentum conservation ? *American Journal of Physics*, 47(7) :583–592, jul 1979.
- A. Jusufi, D. T. Kawano, T. Libby, and R. J. Full. Righting and turning in mid-air using appendage inertia : Reptile tails, analytical models and bio-inspired robots. *Bioinspir. Biomim. 5 045001 Bioinsp. Biomim.*, 5 :45001–12, 2010.
- T. R. Kane and M. P. Scher. A dynamical explanation of the falling cat phenomenon. *International Journal of Solids and Structures*, 5(7) :663–670, 1969.

- I. Kolmanovsky, N. H. McClamroch, and V. T. Coppola. New results on control of multibody systems which conserve angular momentum. *Journal of Dynamical and Control Systems*, 1(4) :447–462, oct 1995.
- T. W. Mather and M. Yim. Modular configuration design for a controlled fall. In *2009 IEEE/RSJ International Conference on Intelligent Robots and Systems*, pages 5905–5910. IEEE, oct 2009.
- M. Reyhanoglu and N. H. McClamroch. Planar reorientation maneuvers of space multibody systems using internal controls. *Journal of Guidance, Control, and Dynamics*, 15(6) :1475–1480, nov 1992.
- C. Rui, I. Kolmanovsky, and N. McClamroch. Control problems for a multibody spacecraft via shape changes : constant nonzero angular momentum. In *Proceedings of the 1997 American Control Conference (Cat. No.97CH36041)*, pages 1904–1908 vol.3. IEEE, 1997.
- C. Rui, I. Kolmanovsky, and N. McClamroch. Nonlinear attitude and shape control of space-craft with articulated appendages and reaction wheels. *IEEE Transactions on Automatic Control*, 45(8) :1455–1469, 2000.
- A. Shapere and F. Wilczek. Gauge kinematics of deformable bodies. *American Journal of Physics*, 57(6) :514–518, jun 1989.
- A. D. Shapere. *Gauge mechanics of deformable bodies*. PhD thesis, University of California, Santa Barbara, 1988.
- J. Wittenburg. *Dynamics of multibody systems*. Springer Science & Business Media, 2007.
- E. C.-Y. Yang, P. C.-P. Chao, and C.-K. Sung. Optimal Control of an Under-Actuated System for Landing With Desired Postures. *IEEE Transactions on Control Systems Technology*, 19(2) :248–255, mar 2011.
- K. Yoshida and Y. Umetani. Control of Space Manipulators with Generalized Jacobian Matrix. pages 165–204. Springer, Boston, MA, 1993.
- J. Zhao, T. Zhao, N. Xi, M. W. Mutka, and L. Xiao. MSU Tailbot : Controlling Aerial Maneuver of a Miniature-Tailed Jumping Robot. *IEEE/ASME Transactions on Mechatronics*, 20(6) :2903–2914, dec 2015.

## Chapitre 2

# Reorientation of a free-floating robot using closed-loop paths in the joint space

### 2.1 Résumé

Cet article présente deux manœuvres distinctes permettant à un robot articulé en chute libre de changer son orientation par le biais de trajectoires fermées dans l'espace articulaire. Il est montré par simulation dynamique que l'amplitude de la rotation nette dépend de l'amplitude du déplacement angulaire des articulations. Avec des limites articulaires réalistes, le robot, qui ne possède que des articulations rototoïdes, est en mesure d'exécuter une rotation de 180 degrés similaire au réflexe de redressement du chat. La seconde manœuvre permet au robot d'accomplir des rotations de moindre amplitude selon un axe différent. Les résultats obtenus en simulation sont validés expérimentalement avec un prototype et un système de capture de mouvements VICON. Enfin, il est montré que le robot peut atteindre n'importe quelle orientation en répétant ou en alternant les manœuvres.

### 2.2 Abstract

This paper presents two distinct manœuvres allowing an articulated robot in free fall to change its orientation using closed-loop paths in the joint space. It is shown through dynamics simulations that the magnitude of the net rotation is dependent upon the amplitude of the angular displacement of the joints. With realistic joint limitations, the robot, which includes rotary actuators only, can perform a 180-degree reorientation about its longitudinal axis, similar to the cat righting reflex. The second manœuvre allows the robot to accomplish rotations of smaller magnitude about a different axis. A physical prototype and a VICON motion tracking system are used to experimentally validate the simulation results. Finally, it

is shown that the robot can reach any orientation by repeating or alternating the manoeuvres.

## 2.3 Introduction

The elusive phenomenon of the self-righting cat falls under the category of problems governed by the law of constant angular momentum. Indeed, with nothing to push against, the cat manages to modify its orientation while free falling, by using the movements of its spine and limbs exclusively. Kane and Scher (Kane and Scher, 1969) were among the firsts to prove that a simplified mathematical model-cat could accomplish a 180 degree flip by executing a specific sequence of movements of the spine. Naturally, several research initiatives in the field of robotics sprouted from the study of this particular phenomenon, and the more general case of reorienting a mechanical system of articulated bodies (Shapere and Wilczek, 1989). As a matter of fact, it is nowadays possible to consider applications where having this ability is not only relevant but essential for a robot. Notably, posture control while falling to mitigate impact for articulated robots was investigated in (Yang et al., 2011; Bingham et al., 2014). Lizard-like self-righting through the use of a tail was studied with simplified systems composed of two bodies in (Jusufi et al., 2010; Chang-Siu et al., 2011; Zhao et al., 2015). Another problem which is closely related to the falling cat phenomenon is the reorientation of humans in free fall. Gymnasts and divers are frequently confronted to this situation as they perform twists and flips in mid-air with zero initial angular momentum (Frohlich, 1979, 1980). Moreover, with the advent of human spaceflight, these manoeuvres were studied extensively (Kulwicki et al., 1962; Smith and Kane, 1967; Kane and Scher, 1970; Stirling, 2008) in order to devise ways for astronauts to change their orientation in weightlessness. However, most of the theoretical research in this area is centred on space systems and satellite control. The ability to control the orientation of multi-body space systems using internal movements could notably reduce the amount of propellant needed and save weight by removing the need for auxiliary systems such as reaction wheels or magnetic torquers. Several modelling methods have been proposed for free-floating space manipulators, like the virtual manipulator approach (Dubowsky and Papadopoulos, 1993) and the generalized Jacobian (Yoshida and Umetani, 1993). Nonlinear control models based on Lie brackets and controllability for this case of nonholonomic problem have also been investigated in depth (Reyhanoglu and McClamroch, 1992; Kolmanovsky et al., 1995; Rui et al., 1997, 2000).

While reproducing weightlessness conditions in 3D space on Earth remains a challenge, several research initiatives have resulted in interesting experimental work. For instance, the results in (Chang-Siu et al., 2013; Wenger et al., 2016) show that a tailed robot can effectively accomplish inertial reorientation. The in-depth analysis of (Libby et al., 2016) concluded that the use of a tail or appendages is particularly interesting for terrestrial robots and also explored the use of flailing limbs. However, although such inertial devices can be effectively integrated in some robot designs, it might not always be possible or desirable to add dedicated appendages such

as multiple-degree-of-freedom (DoF) tails or joints with an infinite range of motion. Moreover, in some cases, these methods take advantage of the fact that the joint trajectories do not form closed loops, i.e., the robot's landing configuration differs from its starting configuration.

In a previous paper, a planar robot that relied on closed-loop movements for reorientation was proposed (Bettez-Bouchard and Gosselin, 2016). However, the planar architecture of the robot still required it to collide with itself to accomplish significant rotations. In practice, robotic manipulators indeed have joint limits to prevent self-collision. One example of a practical robot capable of righting itself in free fall while incorporating joint limitations is presented in (Mather and Yim, 2009). This robot, which is based on Kane and Scher's model, uses a Lie bracket control to generate the desired reorientation, without using appendages. This type of model was also experimentally validated in (Kawamura, 2014). Finally, the effect of the angle of the distal links during a cat-like reorientation was investigated with a practical robot in (Zhao et al., 2017).

This article proposes two manoeuvres for reorienting an articulated robot under zero angular momentum in a weightless environment. Much like the cat motion itself, the method relies on closed paths (loops) in the joint space to produce a net change in orientation. Practically, this means that the change in orientation is not specifically imparted to an end-effector or certain links, but to the robot as a whole. This paper notably distinguishes itself from the current literature on the following aspects. First, as mentioned, it introduces two distinct manoeuvres which each result in a different reorientation. Both manoeuvres are applicable to typical manipulator architectures, and one is particularly effective at generating significant rotation. It is also shown that these manoeuvres can act as motion primitives and can be used as a way of reaching any orientation in 3D space. Finally, this article also proposes a rigorous non-trivial experimental validation method based on quantitative data.

This paper is structured as follows. The proposed reorientation manoeuvres are first described in Section 2.4. Then, the mathematical model, which is based on the conservation of angular momentum, is introduced in Section 2.5. Section 2.6 presents the design of the prototype of an articulated robot on which the proposed manoeuvres are implemented. Simulation results obtained with a dynamic simulation program are then presented in Section 2.7, where the effects of some of the design parameters on the reorientation are studied and discussed. Section 2.8 presents the experimental validation of the manoeuvres using the physical 3-DoF articulated prototype. Section 2.9 elaborates on the implications of having two different reorientation manoeuvres. Finally, conclusions are drawn in Section 2.10.

## 2.4 Rorrientation Manoeuvres

The first proposed manoeuvre (referred to as manoeuvre A) can be decomposed in 6 steps, as shown in Figure 2.1. Transposing this method to the falling cat would imply that the animal

twists its body along the spine axis, as opposed to Kane and Scher's "no-twist" model. There are diverging opinions on whether the cat effectively does so (Frohlich, 1979). However, the manoeuvre is comparable to a "swivel-hips" that trampolinists execute to rotate their body 180 degrees (Frohlich, 1979).

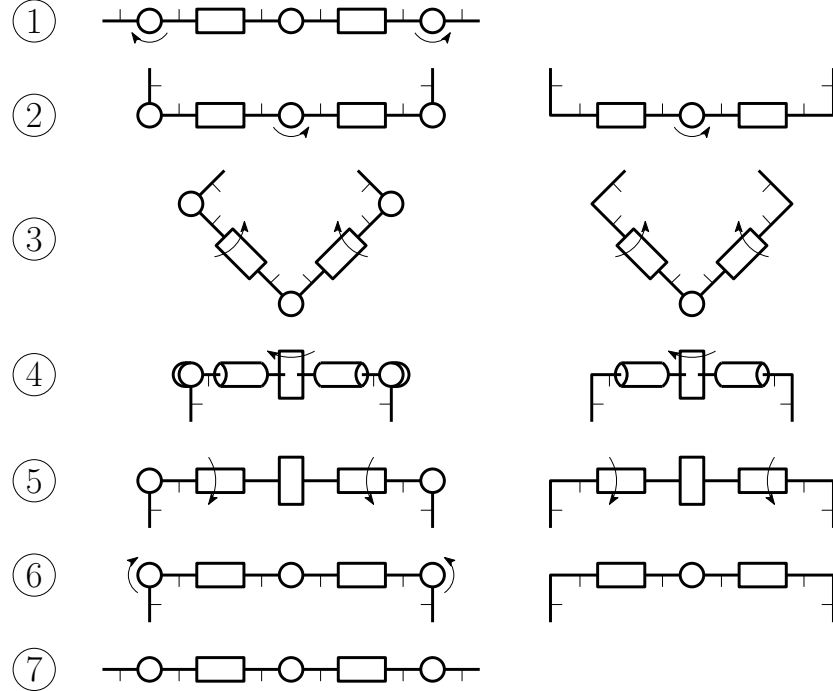


FIGURE 2.1 – Description of manoeuvre A : Manoeuvre steps for a six-body, five-joint architecture (left). Manoeuvre steps for a four-body, three-joint architecture (right). Thinner line stubs show link orientation.

The manoeuvre is well suited for a serial articulated robot composed of six bodies and five rotary actuators. In addition, this architecture does not rely on an actuated Hooke joint, in contrast with other works in the literature that use the "no-twist" model. The system can also be reduced to four bodies and three rotary actuators for simplicity, without notable loss of performance. We can discard steps 1 and 6 and use an "L" shape for the first and last links of the chain, without actuators 1 and 5, as shown in Figure 2.1. This simplifies the experimental process by reducing the number of control inputs and allowing more time for the most important parts of the sequence before the robot touches the ground.

The manoeuvre works by changing the moment of inertia of certain parts of the system between each actuation of the joints. For instance, at step 3, when actuating joint 2 of the six-body system, the moment of inertia (with respect to the joint axis) of the combined bodies to the right of the joint is much larger than the moment of inertia of the bodies to the left. Thus, qualitatively, the left segment will be subject to a large rotation, while the right segment will experience little rotation. By contrast, at step 5, the relative moments of inertia of the left

and right sides are similar, therefore both sides will rotate by a similar amount. This way, the relative angle between each link always returns to its original value at the end of the manoeuvre, effectively meaning that the robot goes back to its starting configuration in the joint space.

A very different reorientation can be obtained by a slight variation of the sequence, while keeping the same robot architecture. As shown in Figure 2.2, by reversing the direction of rotation of joint 1 or joint 3, the robot performs what can be compared to a "signal flag" motion (Kulwicki et al., 1962) (referred to as manoeuvre B). Concretely, this allows for net rotations mainly about the yaw axis of the robot, while manoeuvre A allows for net rotations about the roll axis.

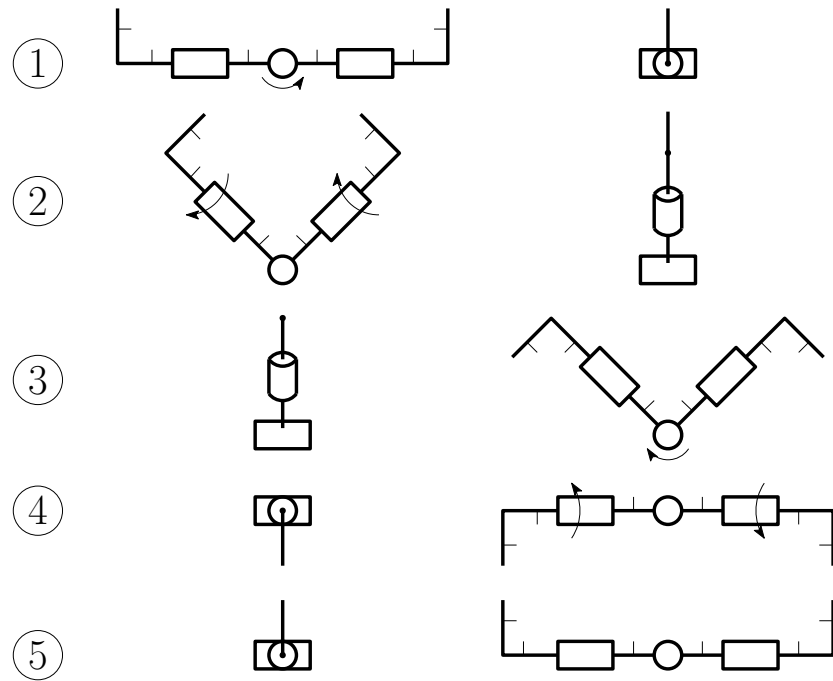


FIGURE 2.2 – Description of manoeuvre B : Front view, manoeuvre steps for a four-body, three-joint architecture (left). Side view, manoeuvre steps for a four-body, three-joint architecture (right). Thinner line stubs show link orientation.

Manoeuvres such as those presented above, when executed in free fall, have the interesting characteristic of being time-independent. In other words, the speed at which the manoeuvre is executed has no impact on the final state of the system : only the geometric path in the joint space matters. A mathematical proof of this property can be found in (Shapere, 1988). Thus, we can use a representation of the paths in joint space without losing significant information, and use this to our advantage for easier parametrization of the trajectories. The proposed manoeuvres for the simplified three-joint architecture are therefore represented as a closed path in the joint space.

## 2.5 Mathematical Background

In order to provide a better understanding of the physics at play during the reorientation, the dynamic model of a free-floating serial robot with  $n$  links and  $j$  revolute joints ( $j = n - 1$ ) is derived in this section. The formulation presented here was proposed in (Bettez-Bouchard and Gosselin, 2016) as an adaptation of (Dubowsky and Papadopoulos, 1993).

Free-floating manipulators differ from their earth-based counterparts in that the position and orientation of each link depend on the position and orientation of every other link in the chain (Wittenburg, 2007). As a consequence of the conservation of momentum, the dynamic behaviour of a free-floating multibody system can be expressed with respect to its global centre of mass ( $CM$ ), as shown in Figure 2.3. Since the position of the  $CM$  is constant in a reference frame  $R_0$  moving with the robot, the position  $\mathbf{r}_i$  and velocity  $\mathbf{v}_i$  of the centre of mass ( $CM_i$ ) of link  $i$  ( $i = 1, \dots, n$ ) is related to that of the other bodies as follows

$$\sum_{i=1}^n m_i \mathbf{r}_i = \mathbf{0}, \quad \sum_{i=1}^n m_i \mathbf{v}_i = \mathbf{0} \quad (2.1)$$

where  $m_i$  is the mass of link  $i$ . Moreover, the conservation of the angular momentum leads to

$$\frac{d\mathbf{h}}{dt} = \mathbf{0}, \quad \mathbf{h} = \sum_{i=1}^n (\mathbf{I}_i \boldsymbol{\omega}_i + m_i \mathbf{r}_i \times \mathbf{v}_i) \quad (2.2)$$

where  $\mathbf{h}$  is the angular momentum,  $\mathbf{I}_i$  is the inertia tensor of link  $i$  and  $\boldsymbol{\omega}_i$  is its angular velocity. As previously stated, it is assumed that the robot is initially at rest ( $\boldsymbol{\omega}_i = \mathbf{v}_i = \mathbf{0}, i = 1, \dots, n$ ) and that no external torque is applied to it during the reorientation, thus  $\mathbf{h}$  is set to  $\mathbf{0}$ .

To compute (2.2), each term must be expressed in the same reference frame, in this case  $R_0$ . The rotation from reference frame  $i - 1$  to reference frame  $i$  can be expressed with matrix  $\mathbf{Q}_i$ . Using an axis angle representation,  $\theta_i$  is the rotation angle about unit vector  $\mathbf{e}_i$  (expressed in its local reference frame) corresponding to the axis of the  $i$ th revolute joint. Matrix  $\mathbf{Q}_1$  corresponds to the rotation from the inertial reference frame to link 1. The representation in  $R_0$  is then obtained by pre-multiplying by the product of rotation matrices  $\mathbf{Q}_1$  to  $\mathbf{Q}_i$  in the case of a vector, and also by post-multiplying by the transpose of these rotation matrices in the case of a tensor.

Next,  $\mathbf{r}_i$ ,  $\mathbf{v}_i$  and  $\boldsymbol{\omega}_i$  must be explicated. The derivation of these terms is based on the concept of barycentre (Wittenburg, 2007), adapted to free-floating serial manipulators in (Bettez-Bouchard and Gosselin, 2016; Dubowsky and Papadopoulos, 1993). For each link, two constant construction vectors are defined, namely  $\underline{\mathbf{r}}_{0i}$  and  $\underline{\mathbf{l}}_{0i}$ , as shown in Figure 2.3. The underscore implies that the vector or tensor is expressed in its local reference frame. Vector  $\underline{\mathbf{r}}_{0i}$  connects  $CM_i$  to joint  $i$ , while vector  $\underline{\mathbf{l}}_{0i}$  connects  $CM_i$  to joint  $i - 1$ .

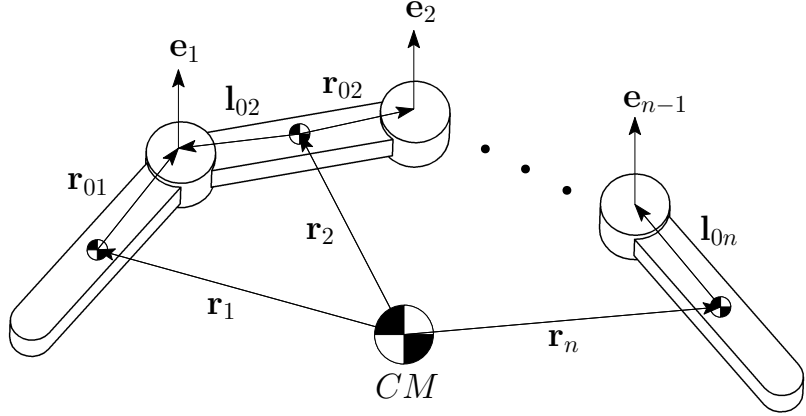


FIGURE 2.3 – Geometric modelling of the robot.

Combining these vectors with the mass of the links yields the position of the barycentre  $\mathbf{c}_{0i}$ , which is given by

$$\mathbf{c}_{0i} = \mathbf{l}_{0i}\mu_i + \mathbf{r}_{0i}(1 - \mu_{i+1}) \quad (2.3)$$

with  $\mu_i$  the mass distribution in the robot, given by

$$\mu_i = \begin{cases} 0 & i = 1 \\ \sum_{k=1}^{i-1} \frac{m_k}{M} & i = 2, \dots, n \\ 1 & i = n+1 \end{cases} \quad (2.4)$$

where  $M$  is the total mass of the robot. Vector  $\mathbf{c}_{0i}$  can equivalently be found by adding a point mass  $M\mu_i$  to joint  $i-1$  and  $M(1-\mu_{i+1})$  to joint  $i$ , which defines an augmented link (Wittenburg, 2007). The barycentre then becomes the centre of mass of this augmented link (Dubowsky and Papadopoulos, 1993). New augmented construction vectors can be defined with respect to this centre of mass, as

$$\underline{\mathbf{c}}_{0i}^* = -\underline{\mathbf{c}}_{0i} \quad (2.5)$$

$$\underline{\mathbf{r}}_{0i}^* = \underline{\mathbf{r}}_{0i} - \underline{\mathbf{c}}_{0i} \quad (2.6)$$

$$\underline{\mathbf{l}}_{0i}^* = \underline{\mathbf{l}}_{0i} - \underline{\mathbf{c}}_{0i}. \quad (2.7)$$

Similarly to vector  $\mathbf{r}_i$ , these vectors are fully specified by the configuration of the robot, which depends on the joint angles collected in vector  $\boldsymbol{\theta}$ . It can be shown that  $\mathbf{r}_i$  can be expressed in terms of the barycentric vectors, which yields

$$\mathbf{r}_i = \sum_{k=1}^n \mathbf{b}_{ki} \quad (2.8)$$

with  $\mathbf{b}_{ki}$  defined using the following rule

$$\mathbf{b}_{ki} = \begin{cases} \mathbf{l}_{0k}^* & k > i \\ \mathbf{c}_{0k}^* & k = i \\ \mathbf{r}_{0k}^* & k < i \end{cases}. \quad (2.9)$$

Vector  $\boldsymbol{\omega}_i$  can be expressed in  $R_0$  by adding the angular velocity vector imparted by each joint with the angular velocity  $\boldsymbol{\omega}_1$  of the first link, which yields

$$\boldsymbol{\omega}_i = \begin{cases} \boldsymbol{\omega}_1 & i = 1 \\ \boldsymbol{\omega}_{i-1} + \mathbf{e}_{i-1}\dot{\theta}_{i-1} & i = 2, \dots, n. \end{cases} \quad (2.10)$$

Considering that vector  $\mathbf{b}_{ki}$  is constant in the reference frame moving with angular velocity  $\boldsymbol{\omega}_i$ ,  $\mathbf{v}_i$  is obtained as

$$\mathbf{v}_i = \sum_{k=1}^n \boldsymbol{\omega}_k \times \mathbf{b}_{ki} \quad i = 1, \dots, n. \quad (2.11)$$

Equation (2.11) can be rearranged with the help of (2.10), yielding

$$\mathbf{v}_i = \boldsymbol{\omega}_1 \times \mathbf{r}_i + \mathbf{C}_i \dot{\boldsymbol{\theta}} \quad (2.12)$$

where  $\mathbf{C}_i$  is a matrix of dimension  $3 \times j$  which is a function of the construction parameters of the robot.

Equations (2.8), (2.10) and (2.12) can now be substituted into (2.2) — where  $\mathbf{h}$  is set to zero — to form a system of equations that depends only on the unknowns  $\boldsymbol{\omega}_1$  and  $\dot{\boldsymbol{\theta}}$ . The double vector product obtained in the process can be rearranged as

$$m_i \mathbf{r}_i \times (\boldsymbol{\omega}_1 \times \mathbf{r}_i) = m_i ((\mathbf{r}_i^T \mathbf{r}_i) \mathbf{1} - \mathbf{r}_i \mathbf{r}_i^T) \boldsymbol{\omega}_1 \quad (2.13)$$

with  $\mathbf{1}$  the identity matrix.

Finally, collecting the terms in  $\boldsymbol{\omega}_1$  on one side and the terms in  $\dot{\boldsymbol{\theta}}$  on the other side, a linear system of equations that relates the angular velocity of the first body and the joint velocity vector of the robot is obtained as

$$\mathbf{A} \boldsymbol{\omega}_1 = \mathbf{B} \dot{\boldsymbol{\theta}} \quad (2.14)$$

where  $\mathbf{A}$  is a  $3 \times 3$  matrix and  $\mathbf{B}$  is a matrix of dimension  $3 \times j$ , which both depend on the mass of the links, the geometric parameters and the configuration of the robot. This formulation of the dynamic model is general and is applicable to any spatial or planar serial free-floating robot.

## 2.6 Prototype Design

Based on the simplified three-joint architecture presented in Section 2.4, an experimental prototype was designed and built. A CAD model of the prototype is shown in Fig 2.4. The robot was designed without any on-board electronics except for the motors themselves. One drawback of this design is that it requires an experimental setup where wires must run between each motor and an external controller for power and encoder signals. The measures that were taken to mitigate the influence of the hanging wires are addressed in more detail in Section 2.8.

The total mass of the robot is approximately 0.3 kg. Machined steel inserts were added to the ends of links 1 and 4 in order to position their centre of mass in a way that favours the reorientation using manoeuvres A and B. Links 2 and 3 are hollow, allowing motors to be mounted inside them. The motors are 4.5 Watt brushed DC *RE-max 17* with 24:1 gearheads and 512 counts per turn encoders.

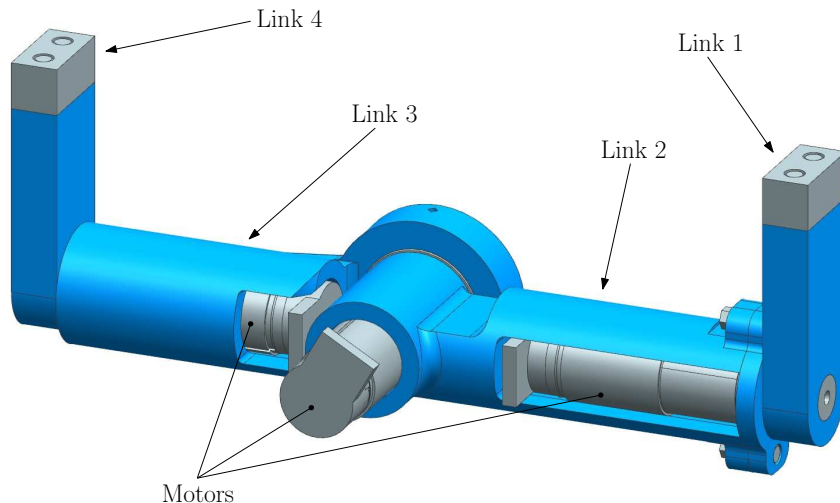


FIGURE 2.4 – CAD model of the prototype. Parts in blue are made of 3D-printed ABS plastic. Parts in grey are made of steel.

## 2.7 Simulation

Using the CAD model, dynamic simulations were performed using Siemens NX to study the effects of various parameters on the dynamics of the robot in zero-gravity. Figure 2.5 shows the progression of manoeuvre A simulated with the CAD model and Figure 2.6 shows the progression of manoeuvre B using the same CAD model.



FIGURE 2.5 – Dynamic simulation of the robot executing manoeuvre A.



FIGURE 2.6 – Dynamic simulation of the robot executing manoeuvre B.

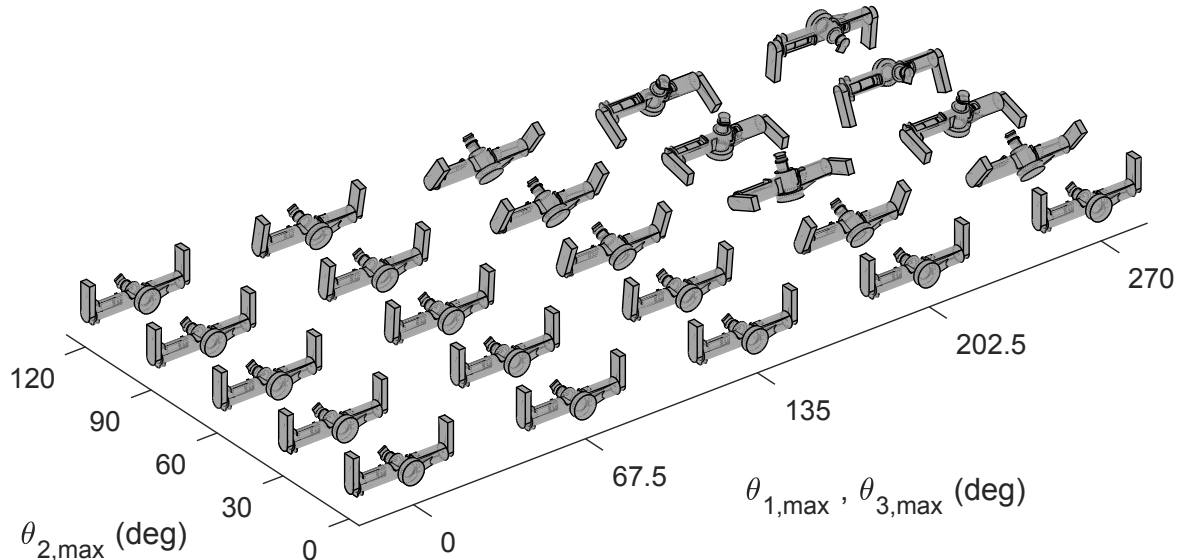


FIGURE 2.7 – Final orientation of the robot after manoeuvre A for different values of maximum joint displacement.

### 2.7.1 Trajectory in the joint space

The influence of the amplitudes of the movements on the net change in orientation, for manoeuvre A, was first investigated. In the joint space, this is equivalent to varying the dimensions of the rectangular loop that represents the trajectory. The final orientation as a function of maximum joint displacement is presented in Figure 2.7.

As it can be observed, the axis describing the net rotation induced by the manoeuvre varies very little with respect to maximum joint displacement. This means that the manoeuvre produces a rotation almost purely about the roll axis of the robot and that undesirable motions around other axes are negligible (almost nonexistent). In addition, the net rotation itself increases smoothly with respect to the maximum movement amplitude of both joints. Therefore, small internal movements of the robot produce a small reorientation while large internal movements

produce a large reorientation, meaning that the manoeuvre behaves predictably. Moreover, with a reasonable displacement limit of 270 degrees for the distal joints and 120 degrees for the centre joint, a net rotation of approximately 180 degrees is predicted by the simulation. For a cat-like reorientation, a half-turn is the worst case scenario, since a rotation of more than 180 degrees is equivalent to a rotation of smaller amplitude in the opposite direction. Practically, rotating in the opposite direction can be done by reversing the direction of rotation of joints 1 and 3.

### 2.7.2 Moment of inertia of the end links

The effect of different inertial parameters on manoeuvre A was also studied. The starting point of this analysis is the realization that drastically increasing the moments of inertia of links 2 and 3 results in no reorientation. Indeed, having bodies 1 and 4 linked to a very high inertia would be comparable to fixing the stators of motors 1 and 3 in space. For this reason, the study was focused on the moment of inertia of links 1 and 4 about joint axes 1 and 3, respectively. Figure 2.8 shows the resulting net rotation for different values of moment of inertia, with the same prescribed joint trajectories for each simulation. For this robot, it can be observed that a moment of inertia of up to approximately  $100 \text{ kg-mm}^2$  contributes to the desired reorientation, that is, a net rotation of 180 degrees. Increasing the inertia past this point has adverse effects on the manoeuvre, notably inducing a progressively greater amount of off-axis rotation and reducing the net amount of rotation about the principal axis of the robot. Moreover, a greater moment of inertia would require higher torques at joints 1 and 3 in order to accomplish the manoeuvre.

### 2.7.3 Motor gear ratio and rotor inertia

With free-floating robots, extra care must be taken in the selection of the motors for joint actuation. Indeed, the motors can significantly influence the dynamic behaviour of the robot in free fall, depending on their properties. For instance, a servomotor with a very high reduction ratio might offer more torque, but its fast spinning rotor may disturb the manoeuvre. To better characterize the influence of the gear ratio and the rotor inertia on manoeuvre A, simulations were performed with different values of these parameters. The results are shown in Figure 2.9.

It can be observed that for this specific manoeuvre and geometric configuration, increasing both the moment of inertia of the rotor and the reduction ratio results in a greater net reorientation. In other words, a smaller maximum displacement at the joints would be sufficient to achieve a net rotation of 180 degrees about the roll axis of the robot. Still, there is a trade-off between performance, form factor, weight and availability of parts, which explains the choice of a 24:1 ratio and rotor inertia of  $0.1 \text{ kg-mm}^2$  for the current robot.

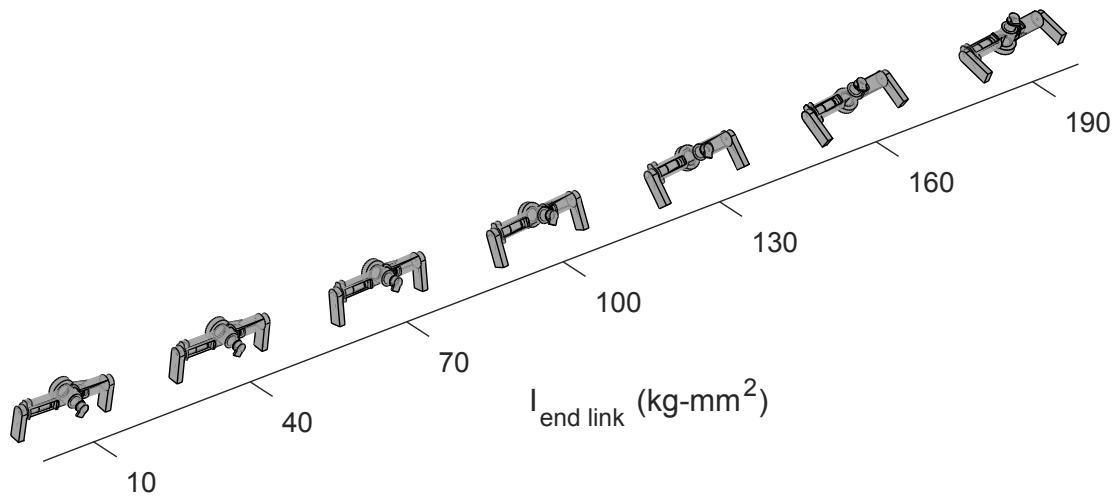


FIGURE 2.8 – Final orientation of the robot after manoeuvre A for different values of moment of inertia of the end links. All simulations are for a maximum displacement of 270 degrees at the distal joints and 120 degrees at the central joint.

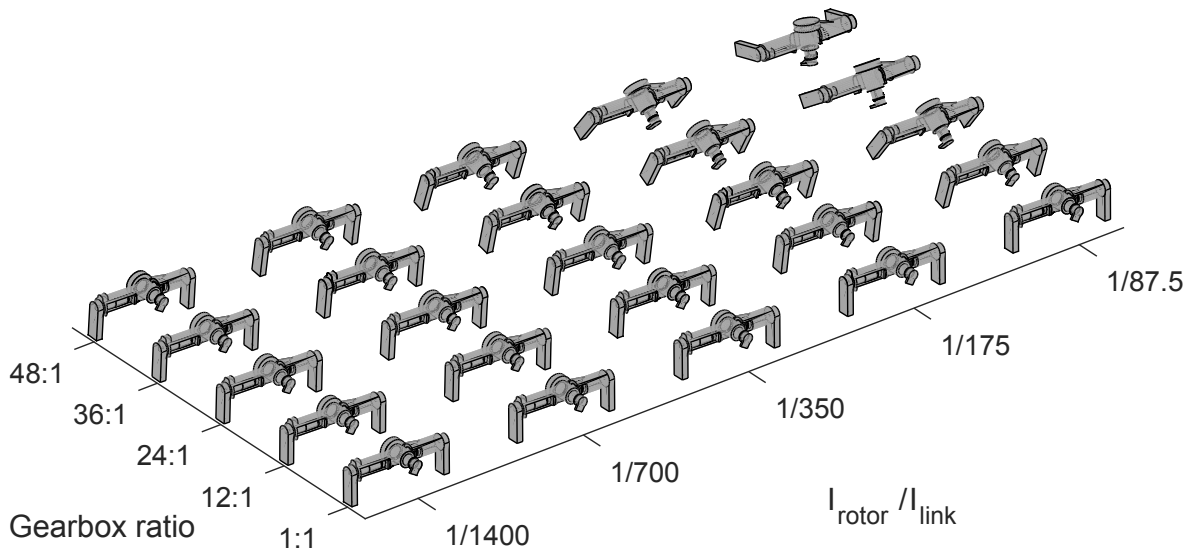


FIGURE 2.9 – Final orientation of the robot after manoeuvre A for different values of rotor inertia and gearbox ratio. All simulations are for a maximum displacement of 270 degrees at the distal joints and 120 degrees at the central joint.

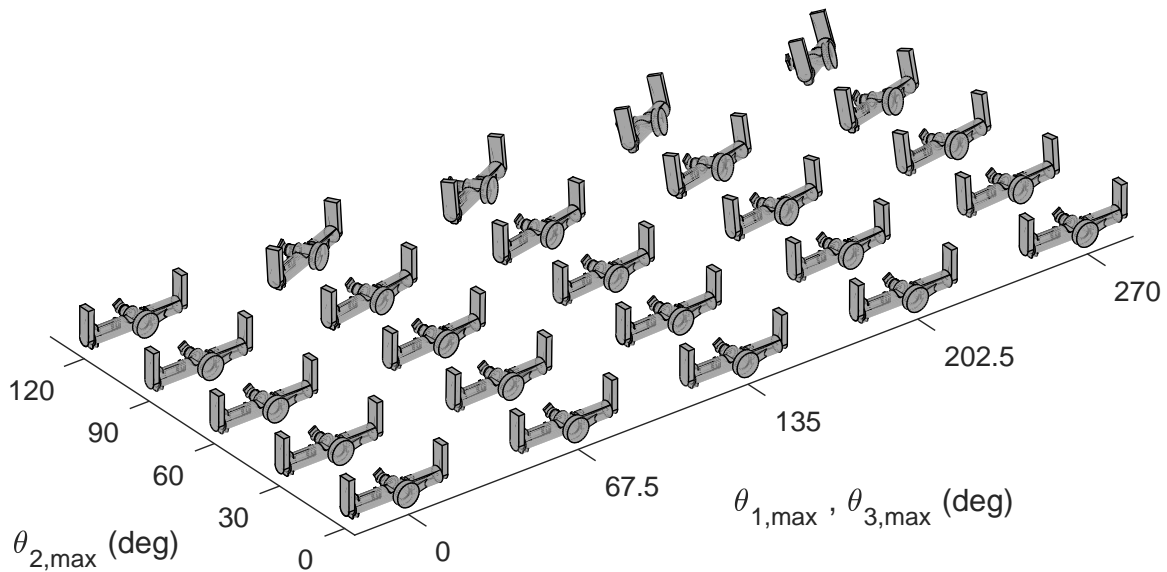


FIGURE 2.10 – Final orientation of the robot after manoeuvre B for different values of maximum joint displacement.

#### 2.7.4 Simulation of Manoeuvre B

The same CAD model was used to carry out simulations for manoeuvre B. The progression of the reorientation for maximum movement amplitudes of  $\theta_{1,max} = 270^\circ$ ,  $\theta_{2,max} = 120^\circ$  and  $\theta_{3,max} = 270^\circ$  is shown in Figure 2.6.

Figure 2.10 shows the net rotation resulting from maximum movement amplitudes ranging from 0 to 270 degrees for  $\theta_1$  and  $\theta_3$  and 0 to 120 degrees for  $\theta_2$ . It can be observed that for the same joint limit ranges, manoeuvre B results in a smaller net rotation than manoeuvre A. This can be attributed to the fact that the robot was designed in a way that rather favours the reorientation with manoeuvre A. Still, the robot accomplishes a maximum rotation of 43 degrees about its yaw axis, with limits of 270 degrees on joints 1 and 3 and 120 degrees on joint 2. However, off-axis rotation is also present, which means that the rotation axis is not aligned with the local axes of the robot.

Finally, similarly to manoeuvre A, there is no holonomy (no net change in orientation) when locking in position the pair of joints 1 and 3 or joint 2 ( $\theta_{i,max} = 0$ ) while executing manoeuvre B. This is because the loop in joint space then degenerates to a line, which also corresponds to the fact that there is no change in the moment of inertia between each actuation of the remaining joint.

## 2.8 Experimental Validation

In order to validate the simulation results, the robotic prototype presented in Section 2.6 was built and an experimental set-up was designed. The prototype is shown in Fig 2.11.



FIGURE 2.11 – Physical prototype with VICON reflective markers.

The drop post shown in the background in Figure 2.12 allows 2 metres of free fall, which is equivalent to approximately 0.6 second of weightlessness. The robot lands in a flexible basket mounted on a damped spring at the end of the drop. In order to limit the influence of initial conditions as much as possible, the release mechanism is a set of two electromagnets. The robot is completely still before release and the manoeuvre only begins 0.02 second after the electrical signal is sent to the electromagnets, to ensure that the robot is effectively released and to prevent any contact with the magnets during the manoeuvre. As mentioned in Section 2.6, the robot has no on-board electronics. To mitigate the influence of the wiring connecting the robot to the controller, the thinnest possible extra flexible silicon insulated wires were used. In addition, a third electromagnet releases the wires simultaneously with the robot. This prevents the wires from pulling on the robot at the instant of release and inducing angular momentum. When the fall is initiated, both the robot and the wires are weightless, thus the manoeuvre is only affected by the relatively small inertia of the wires.

For practical reasons, the drop height is limited. Thus, it is necessary to verify that the motors have enough power to execute the manoeuvre in the allowed time. To this end, the torque and speed values at each time step are extracted from the dynamic simulations of the manoeuvre and compared against the torque-speed limiting curve of the motors provided by the manufacturer. The allotted time for each step of the manoeuvre is then iteratively adjusted

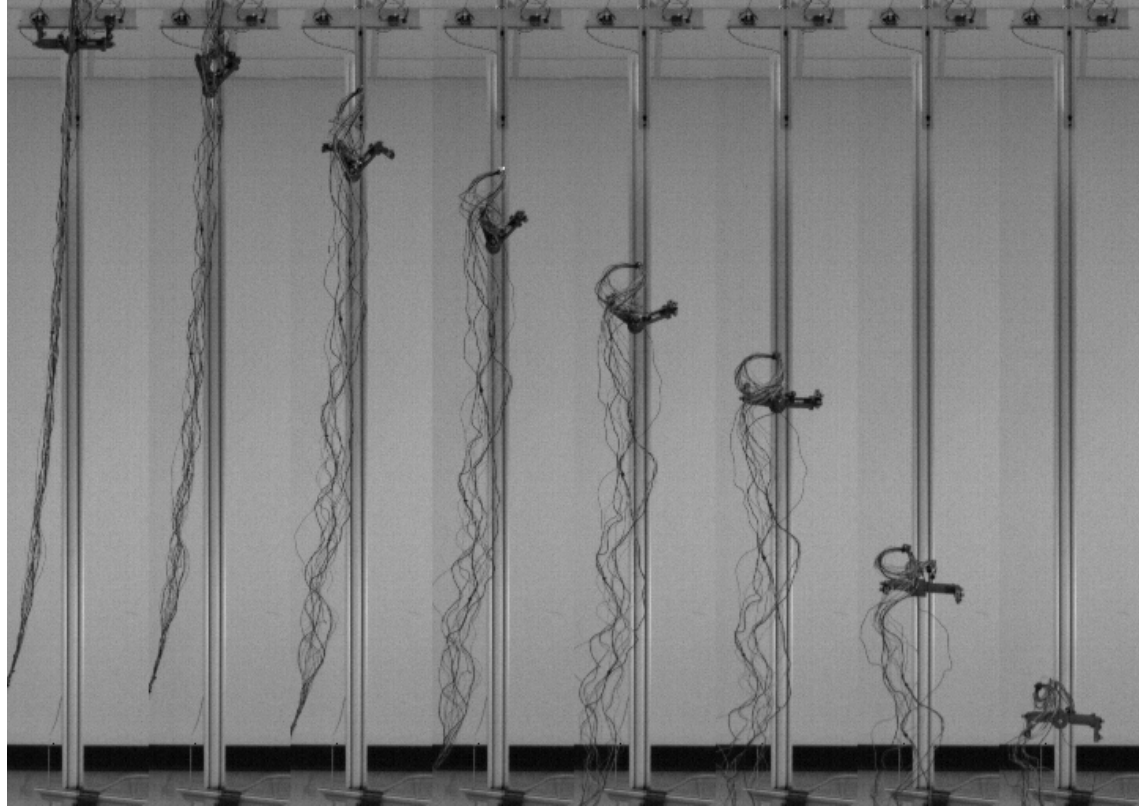


FIGURE 2.12 – Still frames from the high speed footage of the robot executing manoeuvre A.

until a minimum-time trajectory is obtained.

It is important to note that the only control input to this robot is the relative angle between each pair of consecutive links. This means that while joints 1, 2 and 3 follow a prescribed trajectory through the use of a PID position control, the orientation of the robot in 3D space is only observed.

For qualitative analysis, the robot was filmed with a high speed camera at 800 frames per second. Figure 2.12 presents still frames from a typical test drop for manoeuvre A. From these images, it can be observed that the orientation of the robot follows what was predicted by the simulations. The prototype accomplishes a half-turn net rotation at the end of the prescribed sequence of joint movements, even with the wires linked to a fixed controller.

For quantitative validation of the observations, the orientation of the first link of the robot was tracked using a VICON motion capture system at a sampling rate of 300 Hz. The markers that are required for tracking have a negligible mass and were positioned on the body so as not to hinder the manoeuvre. The motion tracker outputs the orientation of the body by fitting a given model to the measurements. Figure 2.13 shows the progression of the orientation with a ZXZ Euler angle representation. It can be clearly observed that the second and third angles

return to their initial value at the end of the fall, while the first angle increases by 3.35 rad. With this convention, the first angle corresponds to the roll axis of the robot. This rotation of just over 180 degrees is what was predicted by the simulation. Figure 2.13 also shows that while joint coordinates did not exactly follow the prescribed curves,  $\theta_1$  and  $\theta_3$  stayed synchronised and each articulation reached the desired angular value at the prescribed time without any overlap between  $\theta_2$  and  $\theta_1$  or  $\theta_3$ . Thus, the data show that the reorientation can be considered successful. Moreover, the experimentally measured orientation of link 1 closely follows the simulation results, with a RMS error of 0.24 rad ( $13.8^\circ$ ) on the first angle, 0.21 rad ( $12^\circ$ ) on the second angle and 0.14 rad ( $8^\circ$ ) on the third angle.

A second experiment was carried out with the same experimental set-up and motion capture capture system, in order to validate manoeuvre B. The results of this trial are displayed in Figure 2.14. As predicted by the simulations, the final net rotation is not purely about a single axis of the robot and thus it affects more than one of the Euler angles with the Euler angle convention used here. Still, the experimental measures tightly follow the predicted simulation values, with overall RMS errors of 0.22 rad ( $12.6^\circ$ ) on angle  $\alpha$ , 0.10 rad ( $5.7^\circ$ ) on angle  $\beta$  and 0.10 rad on angle  $\gamma$ . The outliers that can be observed near the 0.2 second mark on angles  $\beta$  and  $\gamma$  are the result of momentarily occluded markers, leading to a wrong interpretation of the data from the VICON system. The RMS deviations are lower than those obtained with manoeuvre A, for every Euler angle. This suggests that manoeuvre B may be less prone to disturbances induced by the hanging wires, notably because the connectors on the robot point up for the whole duration of the drop, and the wires are not dragged in different directions. By contrast, the last step of manoeuvre A requires a significant movement of the wires.

To summarise, the experimental robot followed the desired joint trajectories and this in turn resulted in a measured change in orientation close to what was predicted in simulation. It is worth restating that these data serve to show that the numerical simulation is valid and that the properties exhibited by the manoeuvres can then be reproduced in real life. The results shown in this section should not be interpreted as a claim on the precision of a reorientation strategy.

## 2.9 Discussion

Two distinct reorientation manoeuvres were elaborated and tested with a robotic prototype. A cat-like manoeuvre achieved a net rotation of a half-turn almost purely about the longitudinal axis of the robot. The other manoeuvre allowed smaller rotations of approximately 43 degrees about a different axis. Both sequences of movements represent loops in the joint space, meaning that the robot returns to its initial configuration, but with a different orientation in space. A key point arising from the ability to rotate about two different local axes is that any orientation can be reached by carefully sequencing these rotations (Lowenthal, 1971; D'Alessandro, 2004;

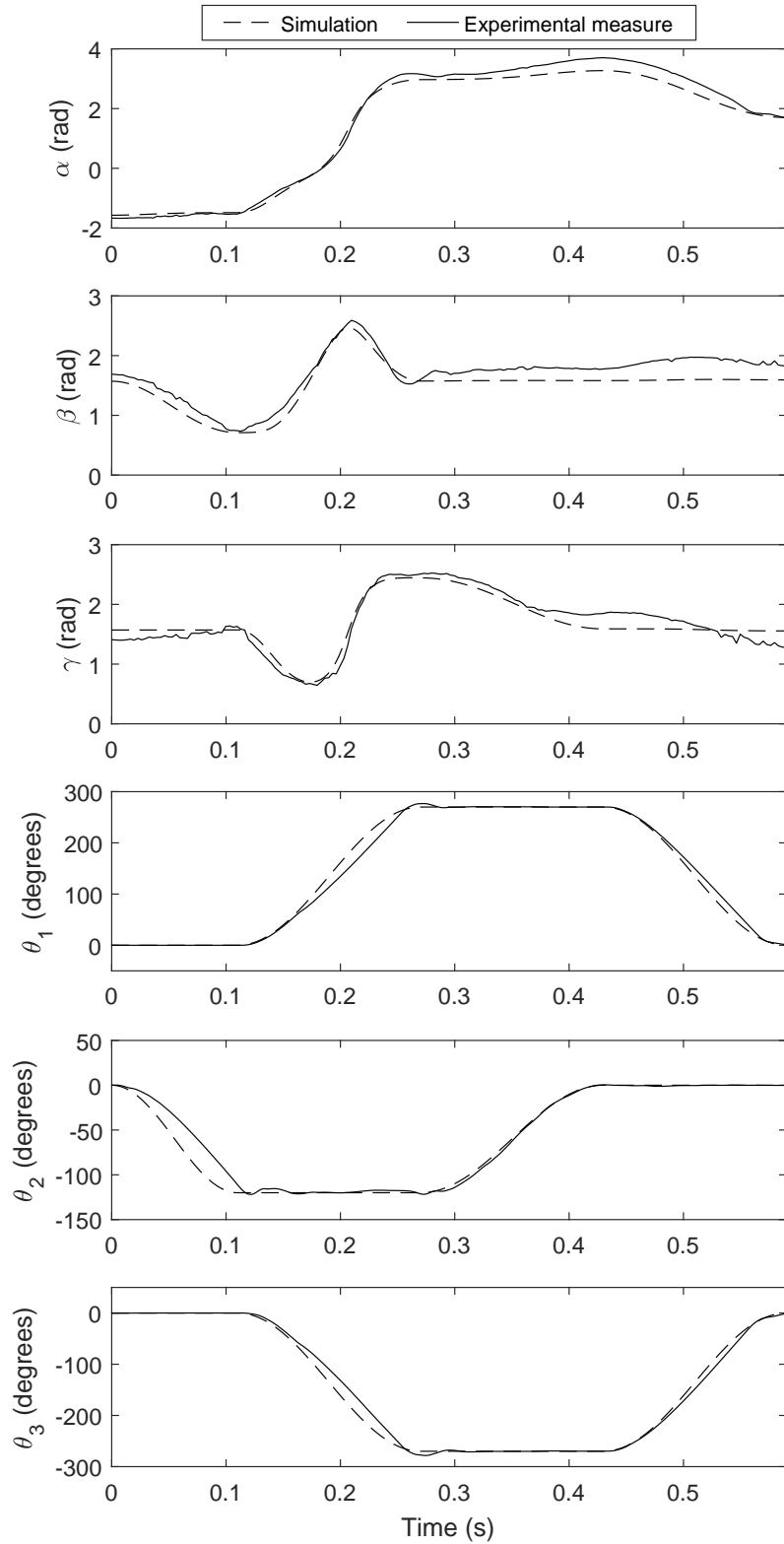


FIGURE 2.13 – Orientation of link 1 in space expressed with Euler angles  $\alpha, \beta, \gamma$  following a ZXZ convention for manoeuvre A. Theoretical and measured joint coordinates for this manoeuvre.

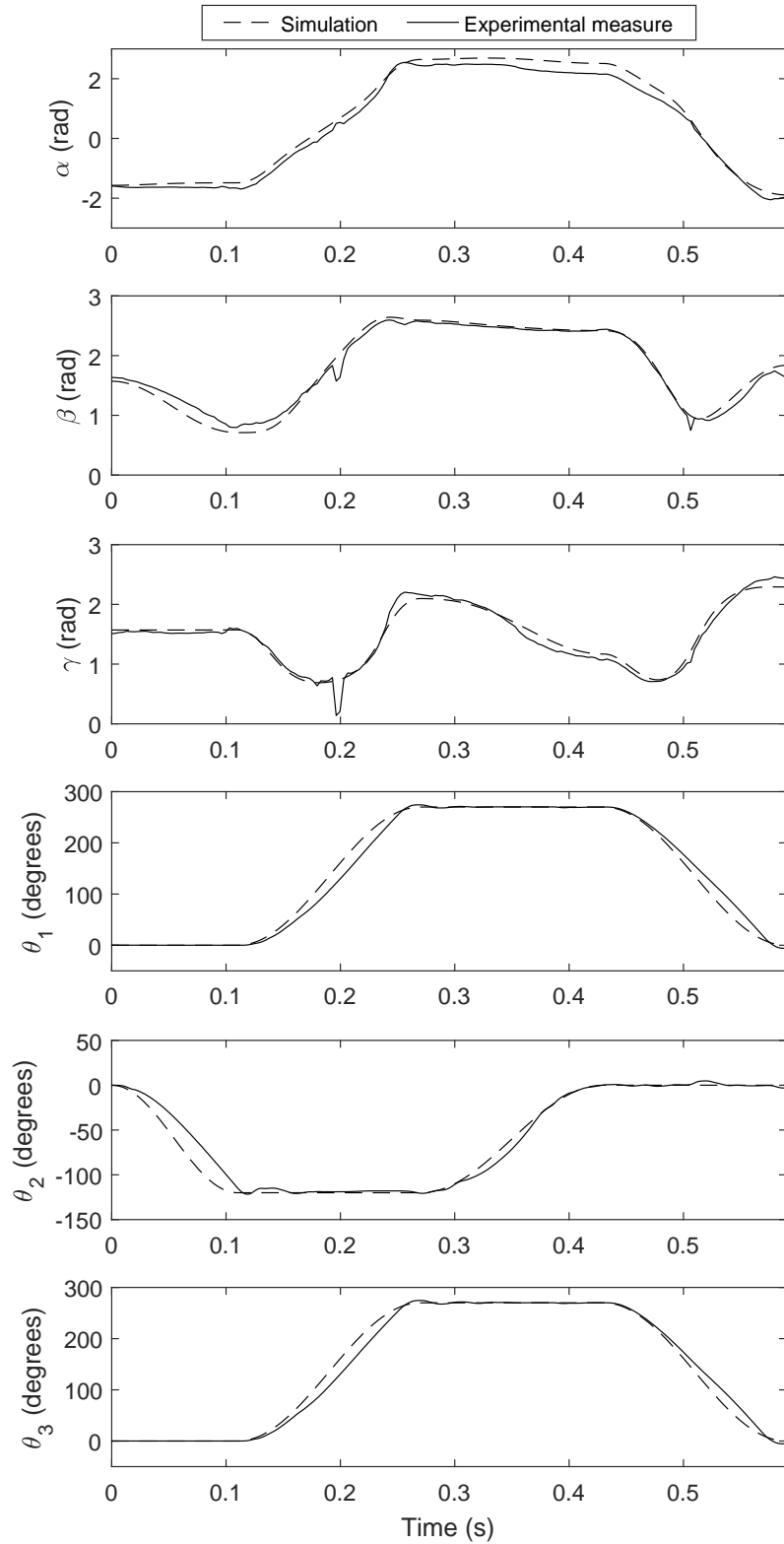


FIGURE 2.14 – Orientation of link 1 in space expressed with Euler angles  $\alpha, \beta, \gamma$  following a ZXZ convention for manoeuvre B. Theoretical and measured joint coordinates for this manoeuvre.



FIGURE 2.15 – Orientation of the robot at the end of each manoeuvre of the sequence.

Hamada, 2014). Moreover, these two axes do not have to be orthogonal, which would be equivalent to any Euler angle convention where the initial axis is repeated as the last axis. However, if the axes are indeed orthogonal, any orientation can be achieved using at most three rotations. These conclusions can be drawn from Lowenthal's formula (Lowenthal, 1971), which can be rewritten (Hamada, 2014) as

$$N = \left\lceil \frac{\pi}{\arccos(\mathbf{m}^T \mathbf{n})} \right\rceil + 1 \quad (2.15)$$

where  $N$  is the required number of alternated rotations about unit axes  $\mathbf{m}$  and  $\mathbf{n}$ ,  $\arccos(\mathbf{m}^T \mathbf{n})$  is the angle between the two axes, and  $\lceil \bullet \rceil$  is the ceiling function. This equation gives an upper bound on the number of rotations needed to achieve *any* orientation, as a function of the angle between the two axes. Other methods exist (D'Alessandro, 2004; Hamada, 2014) in order to find the minimum number of rotations for a *specific* target orientation and the optimal sequence to reach it. In that case, the number of rotations needed may be lower than three.

Lowenthal's formula and the other referenced methods are based on the assumption that an infinite rotation is possible about each axis. This may not always be the case in real life, as it is shown in this article, where specific manoeuvres coupled with joint limits produce a limited rotation. However, a large rotation about a single axis can be decomposed as a repetition of smaller rotations : the same manoeuvre can be repeated any number of times to achieve an arbitrary rotation about a single axis. Obviously, this may not be possible for terrestrial robots in free fall, since time is limited by the height of the fall. Nevertheless, space robots benefit from having a virtually infinite amount of time to accomplish a sequence of manoeuvres. In that case, the movements can also be made arbitrarily slow in order to reduce the required torques at the joints to safe or allowable levels for the robot.

To better illustrate this, a simulated example of a combination of manoeuvres is shown in Figure 2.15. To accomplish this final orientation, manoeuvres A and B are repeated or alternated a total of 6 times. The end result is a net rotation mainly about the pitch axis of the robot, which is not directly feasible using a single manoeuvre with this robot, unlike the previous manoeuvres presented. Moreover, this orientation cannot be reached by repeating manoeuvre A or manoeuvre B alone. However, when combining them, any net rotation can be executed, even if the axes describing the net rotation induced by these manoeuvres are not perfectly orthogonal. In this example, the sequence is defined as follows :

1. Execute manoeuvre B with  $\theta_{1,max} = 270^\circ, \theta_{2,max} = 120^\circ, \theta_{3,max} = 270^\circ$
2. Repeat step 1
3. Execute manoeuvre A with  $\theta_{1,max} = 200^\circ, \theta_{2,max} = 80^\circ, \theta_{3,max} = 200^\circ$
4. Execute manoeuvre B with  $\theta_{1,max} = 270^\circ, \theta_{2,max} = 120^\circ, \theta_{3,max} = 270^\circ$
5. Repeat step 4
6. Execute manoeuvre A with  $\theta_{1,max} = 120^\circ, \theta_{2,max} = 120^\circ, \theta_{3,max} = 120^\circ$

where the sixth step only serves to compensate for the accumulated orientation error, due to the off-axis rotation induced by manoeuvre B. Numerically, the net rotation from the initial orientation of the robot to its final orientation is then

$$\mathbf{R} = \begin{bmatrix} -0.0197 & 0.0411 & -0.9990 \\ -0.1666 & 0.9858 & 0.0438 \\ 0.9858 & 0.1673 & -0.0126 \end{bmatrix} \quad (2.16)$$

while an ideal pure rotation of -90 degrees about the pitch axis of the robot would be given by

$$\mathbf{R}_{ideal} = \begin{bmatrix} 0 & 0 & -1 \\ 0 & 1 & 0 \\ 1 & 0 & 0 \end{bmatrix}. \quad (2.17)$$

The above sequence is roughly equivalent to the following ideal sequence :

1. Rotate 90 degrees about the yaw axis of the robot
2. Rotate 90 degrees about the roll axis of the robot
3. Rotate 90 degrees about the yaw axis of the robot

These results imply that, provided that enough time is allowed, a terrestrial robot could land on its legs at the end of a fall, even with a completely arbitrary starting orientation. It is also interesting to note that, although the robot presented here was not specifically designed to achieve arbitrary rotations, it is able to do so. Moreover, this robot can accomplish such arbitrary rotations using only three rotary actuators.

## 2.10 Conclusion

Two reorientation manoeuvres were elaborated and tested with a robotic prototype. The cat-like movement sequence achieved a net rotation of a half-turn almost purely about the roll axis of the robot. The other manoeuvre allowed a maximum rotation of 43 degrees, mainly about the yaw axis of the robot. Furthermore, the manoeuvres proved stable with respect to maximum joint displacement. That is, lowering the limits on either the central or distal joints only resulted in a smaller net rotation about the same axis. Thus, a large rotation about a single axis can be performed using a repetition of smaller rotations : the same manoeuvre

can be repeated any number of times to achieve an arbitrary rotation about a single axis. Admittedly, this may not always be possible for terrestrial robots in free fall, since time is limited by the height of the fall. Nevertheless, the proposed technique can be used for space robots, where the time taken to accomplish the manoeuvre is not a limitation and where motions can be performed very slowly in order to reduce the required joint torques and ensure safety.

It is also worth restating that the presented proof of concept prototype was originally designed with the intent of validating manoeuvre A. Still, the two manoeuvres lend themselves to a typical 7-DoF shoulder-elbow-wrist serial manipulator architecture. This type of serial robot is frequent in space applications and notable examples include Canadarm2, the European Robotic Arm and the DARPA FREND arm (Flores-Abad et al., 2014). Also, terrestrial walking or jumping robots can be envisioned based on this architecture and it is interesting to note that no special or dedicated appendages were used here for reorientation.

A limitation of our study is that the proposed manoeuvres only work as intended in the absence of angular momentum. If the robot already has angular momentum, moving its links can result in off-axis spins that are more complex to predict, such as when a diver performs a twisting somersault (Frohlich, 1979). Additionally, as the robot used in this work for the experimental validation is a proof of concept, only the motors in the joints of the robot are controlled in closed-loop. This means that the orientation of the robot in space is only controlled in open-loop. As previously stated, there are no on-board electronics, hence no sensors for feedback and reaction to disturbances. Consequently, future work will notably consist in integrating sensors providing information on the orientation of the robot. Incorporating this information in the control loop will enable the development of methods which allow the robot to react to external disturbances. Moreover, the automation of the synthesis of more complex sequences using basic manoeuvres, such as the one presented in Section 2.9, will also be the subject of future work.

## 2.11 Bibliographie

- J.-A. Bettez-Bouchard and C. Gosselin. Development and experimental validation of a re-orientation algorithm for a free-floating serial manipulator. In *2016 IEEE International Conference on Robotics and Automation (ICRA)*, pages 2733–2738. IEEE, may 2016.
- J. T. Bingham, J. Lee, R. N. Haksar, J. Ueda, and C. K. Liu. Orienting in mid-air through configuration changes to achieve a rolling landing for reducing impact after a fall. In *2014 IEEE/RSJ International Conference on Intelligent Robots and Systems*, pages 3610–3617. IEEE, sep 2014.
- E. Chang-Siu, T. Libby, M. Tomizuka, and R. J. Full. A lizard-inspired active tail enables rapid

- maneuvers and dynamic stabilization in a terrestrial robot. In *2011 IEEE/RSJ International Conference on Intelligent Robots and Systems*, pages 1887–1894. IEEE, sep 2011.
- E. Chang-Siu, T. Libby, M. Brown, R. J. Full, and M. Tomizuka. A nonlinear feedback controller for aerial self-righting by a tailed robot. In *2013 IEEE International Conference on Robotics and Automation*, pages 32–39. IEEE, may 2013.
- D. D’Alessandro. Optimal evaluation of generalized Euler angles with applications to control. *Automatica*, 40(11) :1997–2002, nov 2004.
- S. Dubowsky and E. Papadopoulos. The kinematics, dynamics, and control of free-flying and free-floating space robotic systems. *IEEE Transactions on Robotics and Automation*, 9(5) :531–543, 1993.
- A. Flores-Abad, O. Ma, K. Pham, and S. Ulrich. A review of space robotics technologies for on-orbit servicing. *Progress in Aerospace Sciences*, 68 :1–26, jul 2014.
- C. Frohlich. Do springboard divers violate angular momentum conservation? *American Journal of Physics*, 47(7) :583–592, jul 1979.
- C. Frohlich. The Physics of Somersaulting and Twisting. *Scientific American*, 242 :154–165, 1980.
- M. Hamada. The minimum number of rotations about two axes for constructing an arbitrarily fixed rotation. *Royal Society open science*, 1(3) :140145, nov 2014.
- A. Jusufi, D. T. Kawano, T. Libby, and R. J. Full. Righting and turning in mid-air using appendage inertia : Reptile tails, analytical models and bio-inspired robots. *Bioinspir. Biomim.* 5 045001 *Bioinsp. Biomim.*, 5 :45001–12, 2010.
- T. Kane and M. Scher. Human self-rotation by means of limb movements. *Journal of Biomechanics*, 3(1) :39–49, jan 1970.
- T. R. Kane and M. P. Scher. A dynamical explanation of the falling cat phenomenon. *International Journal of Solids and Structures*, 5(7) :663–670, 1969.
- T. Kawamura. Understanding of Falling Cat Phenomenon and Realization by Robot. *Journal of Robotics and Mechatronics*, 26(6) :685–690, dec 2014.
- I. Kolmanovsky, N. H. McClamroch, and V. T. Coppola. New results on control of multibody systems which conserve angular momentum. *Journal of Dynamical and Control Systems*, 1 (4) :447–462, oct 1995.
- P. V. Kulwicki, E. J. Schlei, and P. L. Vergamini. Weightless man : Self-rotation techniques. Technical report, Air Force Aerospace Medical Research Lab, 1962.

- T. Libby, A. M. Johnson, E. Chang-Siu, R. J. Full, and D. E. Koditschek. Comparative Design, Scaling, and Control of Appendages for Inertial Reorientation. *IEEE Transactions on Robotics*, 32(6) :1380–1398, dec 2016.
- F. Lowenthal. Uniform finite generation of the rotation group. *Rocky Mountain Journal of Mathematics*, 1(4) :575–586, dec 1971.
- T. W. Mather and M. Yim. Modular configuration design for a controlled fall. In *2009 IEEE/RSJ International Conference on Intelligent Robots and Systems*, pages 5905–5910. IEEE, oct 2009.
- M. Reyhanoglu and N. H. McClamroch. Planar reorientation maneuvers of space multibody systems using internal controls. *Journal of Guidance, Control, and Dynamics*, 15(6) :1475–1480, nov 1992.
- C. Rui, I. Kolmanovsky, and N. McClamroch. Control problems for a multibody spacecraft via shape changes : constant nonzero angular momentum. In *Proceedings of the 1997 American Control Conference (Cat. No.97CH36041)*, pages 1904–1908 vol.3. IEEE, 1997.
- C. Rui, I. Kolmanovsky, and N. McClamroch. Nonlinear attitude and shape control of spacecraft with articulated appendages and reaction wheels. *IEEE Transactions on Automatic Control*, 45(8) :1455–1469, 2000.
- A. Shapere and F. Wilczek. Gauge kinematics of deformable bodies. *American Journal of Physics*, 57(6) :514–518, jun 1989.
- A. D. Shapere. *Gauge mechanics of deformable bodies*. PhD thesis, University of California, Santa Barbara, 1988.
- P. G. Smith and T. R. Kane. The Reorientation of a Human Being in Free Fall. 1967.
- L. A. Stirling. Development of astronaut reorientation methods : a computational and experimental study. 2008.
- G. Wenger, A. De, and D. E. Koditschek. Frontal plane stabilization and hopping with a 2DOF tail. In *2016 IEEE/RSJ International Conference on Intelligent Robots and Systems (IROS)*, pages 567–573. IEEE, oct 2016.
- J. Wittenburg. *Dynamics of multibody systems*. Springer Science & Business Media, 2007.
- E. C.-Y. Yang, P. C.-P. Chao, and C.-K. Sung. Optimal Control of an Under-Actuated System for Landing With Desired Postures. *IEEE Transactions on Control Systems Technology*, 19(2) :248–255, mar 2011.
- K. Yoshida and Y. Umetani. Control of Space Manipulators with Generalized Jacobian Matrix. pages 165–204. Springer, Boston, MA, 1993.

J. Zhao, T. Zhao, N. Xi, M. W. Mutka, and L. Xiao. MSU Tailbot : Controlling Aerial Maneuver of a Miniature-Tailed Jumping Robot. *IEEE/ASME Transactions on Mechatronics*, 20(6) :2903–2914, dec 2015.

J. Zhao, L. Li, and B. Feng. Effect of swing legs on turning motion of a free-falling cat robot. In *2017 IEEE International Conference on Mechatronics and Automation (ICMA)*, pages 658–664. IEEE, aug 2017.

# Chapitre 3

## Méthodologie

Ce chapitre expose dans un premier temps la méthodologie utilisée pour le volet simulation des travaux de recherche. Le modèle dynamique utilisé en simulation est d'abord détaillé. Par la suite, les différents cas d'utilisation de la simulation ainsi que les processus pour arriver aux résultats finaux sont décrits. Dans un deuxième temps, la méthode expérimentale est présentée. Le montage physique permettant de mener à bien les expériences est décrit, puis le fonctionnement du système Vicon ainsi que les raisons qui ont motivé son utilisation sont expliqués.

### 3.1 Simulation numérique

La simulation numérique a été la première étape du volet de collecte de données pour les travaux de recherche dans ce mémoire.

À partir du modèle 3D du robot réalisé avec un logiciel de CAO, un modèle mécanique du prototype a pu être créé à l'aide du logiciel Siemens NX. Ce modèle, qui sert ultimement à exécuter des simulations dynamiques, incorpore notamment des informations sur la masse et l'inertie des corps rigides inclus dans la simulation. Le type d'articulation (rotoïde, prismatique, sphérique, etc.) reliant chaque corps, ainsi que le type d'actionnement (articulation passive ou active) font aussi partie des informations principales incluses dans le modèle. Concrètement donc, le modèle dynamique comporte quatre corps rigides, représentant les membrures du robot, reliés par trois articulations rotoïdes actives. Les rotors des moteurs sont aussi inclus dans le modèle, avec la contrainte de suivre une vitesse angulaire 24 fois supérieure à celle des articulations, pour représenter l'effet des réducteurs 24:1 installés sur les moteurs.

Pour le prototype à l'étude dans ce travail, les entrées du modèle sont donc les trajectoires suivies par les articulations dans l'espace articulaire. Dans le cas présent, ceci correspond au déplacement angulaire, puisque le robot ne possède que trois articulations rotoïdes. Les sorties du modèle sont le couple requis aux articulations ainsi que la position et l'orientation de chaque

membrure du robot, pour chaque pas de temps.

Siemens NX permet aussi d'exporter le modèle comme une simple boîte dans le logiciel Simulink, ce qui donne alors accès à l'environnement MATLAB. Dans ce cas, le modèle Simulink agit comme intermédiaire entre MATLAB et Siemens NX, tel que montré à la Figure 3.1. Ainsi, différents programmes MATLAB ont été élaborés dans le but de mener à bien les différentes tâches nécessitant des simulations dynamiques.

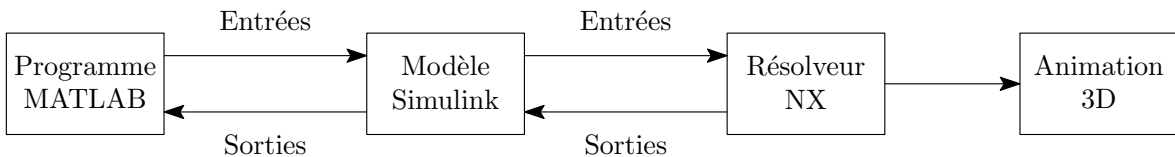


FIGURE 3.1 – Schéma du processus de simulation.

Premièrement, un programme MATLAB permet d'automatiser la prise de données de simulation pour étudier l'effet de l'amplitude de mouvement sur la réorientation. Ce programme se charge d'itérer sur les paramètres d'entrée de la simulation numérique, c'est-à-dire qu'il lance la simulation numérique avec des trajectoires articulaires dont l'amplitude croît à chaque itération jusqu'à une limite imposée. Le programme récupère en sortie l'orientation de la première membrure du robot et enregistre l'information dans une structure de données, qui sera utilisée pour la présentation des résultats. Le même processus est utilisé pour étudier l'effet de paramètres qui modifient le comportement dynamique du robot sur le résultat final de la réorientation. Ainsi, un second programme permet de modifier des valeurs telles que certains moments d'inertie ou les rapports de réduction des moteurs entre chaque itération de la simulation.

Deuxièmement, afin de mener à bien les essais expérimentaux, il est primordial de valider que les moteurs soient assez puissants pour exécuter les trajectoires articulaires dans un temps imparti. Puisque les moteurs utilisés sont des moteurs à courant continu à balais, on peut facilement déterminer leur droite limite dans un graphique couple-vitesse à partir des données du fabricant. À partir de la simulation numérique, il est aussi possible d'extraire les données de couple et de vitesse pour chaque articulation, à chaque pas de temps, afin de générer les courbes couple-vitesse qui résultent de la manœuvre de réorientation. Ainsi, du moment où ces courbes sont inférieures à la fois à la droite limite des moteurs et à la limite de couple des réducteurs, la manœuvre est faisable. Pour trouver le temps minimal nécessaire au robot pour exécuter la manœuvre, un programme MATLAB démarre avec un estimé initial de temps pour chaque étape de la manœuvre, puis compare les courbes couple-vitesse obtenues avec la simulation aux courbes limites des moteurs. Puisque le temps a une influence directe sur les couples et les vitesses, celui-ci est ajusté itérativement jusqu'à atteindre la limite des moteurs. Un exemple de ce processus est montré à la Figure 3.2.

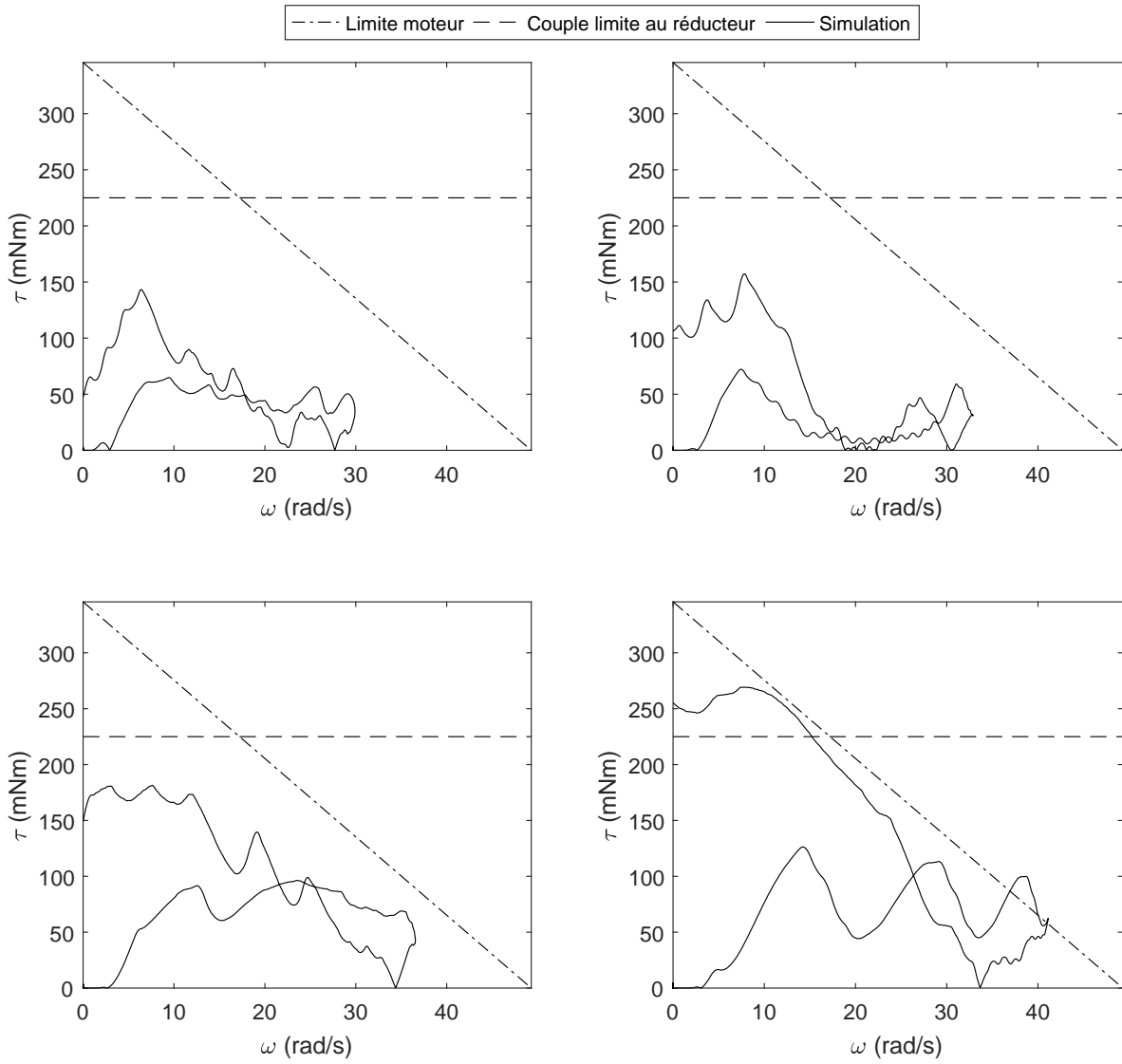


FIGURE 3.2 – Courbes couple-vitesse pour l’articulation centrale, pour la première étape de la manoeuvre. Coin supérieur gauche : Durée de 110 ms, moteur sous-utilisé. Coin supérieur droit : Durée de 100 ms, moteur sous-utilisé. Coin inférieur gauche : Durée de 90 ms, moteur utilisé efficacement. Coin inférieur droit : Durée de 80 ms, moteur sur-utilisé.

### 3.2 Validation expérimentale

Afin de valider les résultats obtenus en simulation, une campagne d’essais expérimentaux a été mise en oeuvre.

### 3.2.1 Éléments physiques du montage

Il existe peu de moyens pour recréer des conditions d'apesanteur sur Terre. Dans le cas d'un robot plan, l'une des techniques les plus simples consiste à placer ce dernier sur un coussin d'air afin d'éliminer la friction avec le plan de travail (à toutes fins pratiques). Toutefois, comme son nom l'indique, le robot plan est contraint de se mouvoir en deux dimensions seulement, ce qui peut constituer une importante restriction. En l'occurrence, les manœuvres de réorientation présentées dans ce mémoire sont impossibles à réaliser en deux dimensions et découlent directement de la structure tridimensionnelle du robot.

Les astronautes en formation pour des sorties à l'extérieur de la station spatiale utilisent quant à eux le principe de flottabilité neutre lors de leurs entraînements. Autrement dit, leur poids est ajusté afin d'être en équilibre avec la poussée d'Archimède exercée par l'eau. Ceci leur permet d'approximer l'effet de l'apesanteur dans un très grand volume, sans être limité par le temps. Toutefois, dans le cas présent, puisque la traînée dans l'eau est beaucoup plus grande que dans l'air, on ne peut poser l'hypothèse qu'aucune force externe n'est appliquée sur le robot. Par ailleurs, le centre de masse d'un robot articulé se déplace de façon non négligeable par rapport à son barycentre géométrique dès que des mouvements sont commandés. Ainsi, même si l'on commande des vitesses très lentes pour négliger la traînée de l'eau, puisque la poussée s'applique au barycentre et l'attraction gravitationnelle au centre de masse, il y aurait pratiquement constamment un couple externe appliqué sur le robot.

Il reste finalement les méthodes ayant recours à une chute libre plus ou moins longue, telle que l'expérimentation sur la Station Spatiale Internationale, le vol parabolique ou la tour d'apesanteur. Bien entendu, les deux premières méthodes sont beaucoup plus difficiles à mettre en œuvre et nécessitent des ressources importantes. Le principe de la tour d'apesanteur n'implique que de laisser tomber la charge utile en chute libre à partir d'une hauteur donnée, ce paramètre étant celui qui détermine le temps de chute. Le principal compromis associé à cette méthode est le temps très limité de chute imposé par l'accélération gravitationnelle. Ce compromis a été jugé acceptable et cette méthode a été retenue.

L'élément central du montage expérimental est donc un poteau d'une hauteur légèrement supérieure à deux mètres, que l'on peut voir en arrière plan à la Figure 1.8. Cette grandeur est limitée, d'une part, par la hauteur normale du plafond d'une pièce intérieure et, d'autre part, par la capacité à amortir l'impact du robot à la fin de la chute. Au sommet du poteau se situe le système de déclenchement, comme le montre la Figure 3.3. Tel que mentionné à la section 1.8, deux des trois électroaimants servent à relâcher le robot, alors que le troisième sert à relâcher les câbles électriques. Puisque des masselottes en acier sont fixées aux extrémités des membrures distales du robot, ce dernier reste accroché au déclencheur jusqu'à ce que le courant soit coupé. À la fin de sa chute, le robot est amorti dans un panier en filet flexible attaché au pied du poteau par un ressort, tel que montré à la Figure 3.3.

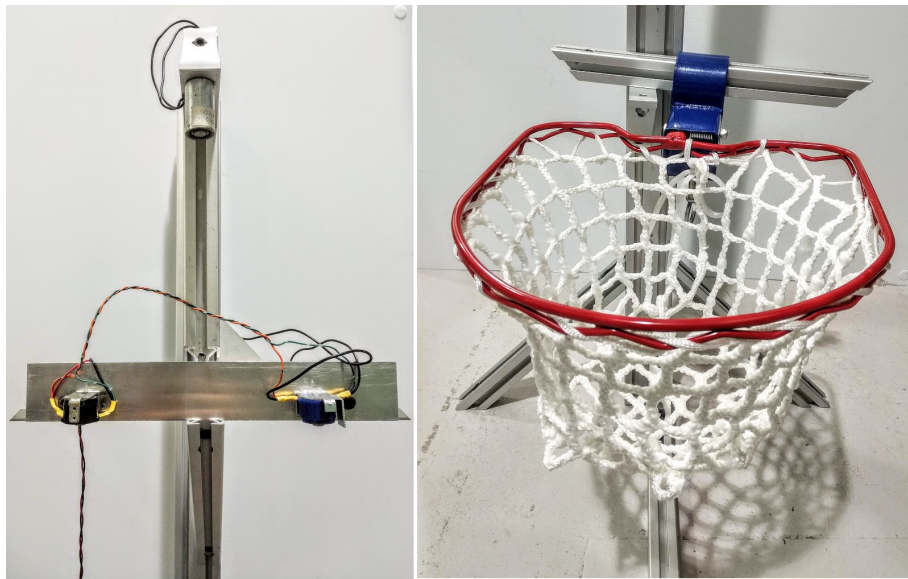


FIGURE 3.3 – Détail du montage expérimental. À gauche : Détail du système de déclenchement. À droite : Détail du panier servant à la réception du robot.

### 3.2.2 Électronique et commande

Le montage électronique permettant de contrôler les moteurs du robot et d'assurer l'actionnement des électroaimants est schématisé à la Figure 3.4. Pour commencer, le programme de contrôle et l'interface utilisateur sont conçus à l'aide de la plateforme RT-Lab, qui utilise l'environnement Simulink. Par la suite, ce programme est converti en langage de bas niveau et transféré dans un ordinateur dont le système d'exploitation fonctionne en temps réel (QNX). Ceci est nécessaire pour assurer le contrôle des moteurs à la fréquence d'échantillonnage demandée. Finalement, l'ordinateur temps réel communique avec une boîte d'amplificateurs pour envoyer la commande aux moteurs et recevoir les signaux.

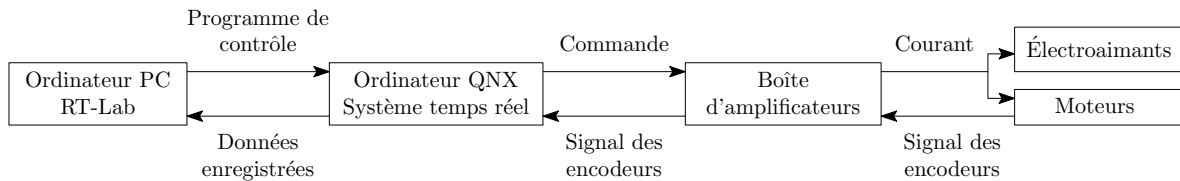


FIGURE 3.4 – Diagramme de fonctionnement de la partie électronique du montage expérimental

L'interface utilisateur permet, entre autres choses, d'envoyer des commandes telles que l'activation de l'alimentation des moteurs ou le lancement de trajectoires articulaires préprogrammées. Dès que l'alimentation des moteurs est activée, un asservissement basé sur un contrôleur de type PID s'assure que les moteurs suivent la consigne de position commandée.

Aux Chapitres 1 et 2, il a été expliqué que la vitesse à laquelle les manœuvres sont exécutées

n'influe pas sur le résultat final de la réorientation. Ainsi, à première vue, il peut paraître vain d'imposer aux articulations des trajectoires de position angulaire en fonction du temps. Toutefois, la synchronisation du mouvement des différentes membrures est d'une importance capitale au bon fonctionnement de la réorientation. Il n'est donc pas suffisant que chaque articulation suive une trajectoire définie, il faut aussi que ces trajectoires suivent une référence commune de temps.

Lors des premiers tests expérimentaux, il a été observé qu'un simple contrôleur PID en position n'était pas assez réactif pour suivre les trajectoires désirées aux articulations. Pour remédier à ce problème, une stratégie de commande de type couples pré-calculés a été implantée dans le programme RT-Lab. Il existe de nombreuses variantes de ce type de commande. Dans le cas présent, la méthode utilisée est inspirée de (Koivo, 1989) et fait appel à deux contrôleurs qui agissent en parallèle sur la commande en couple, tel que montré à la Figure 3.5. Dans cette figure,  $\theta_d$  est le vecteur des positions angulaires désirées et  $\theta$  est le vecteur des positions angulaires réelles.  $\tau_c$  est le vecteur des couples articulaires calculé avec le modèle dynamique du robot et  $\tau_u$  est le vecteur des couples articulaires résultant de la loi de commande PID.

Par définition, une simple loi de commande PID doit forcément attendre d'accumuler une certaine erreur avant d'agir sur la commande envoyée. Certes, ce comportement peut être ajusté en fonction des gains imposés au contrôleur. Malgré cela, notamment dans le cas de trajectoires très dynamiques, il est possible que la réponse du robot demeure insatisfaisante. En ce sens, la commande par couples pré-calculés est intéressante dans la mesure où elle dicte une valeur de couple de référence dès le premier instant de la trajectoire et jusqu'à sa fin.

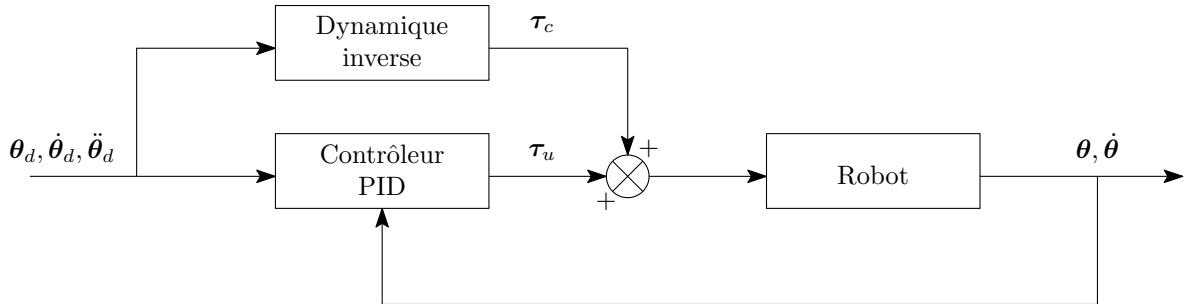


FIGURE 3.5 – Schéma de commande par couples pré-calculés.

La dynamique inverse consiste à calculer, à partir du modèle dynamique du robot, les couples théoriques nécessaires pour obtenir les valeurs articulaires désirées. Certaines hypothèses peuvent être posées pour simplifier grandement ce calcul.

Le modèle dynamique général d'un manipulateur est donné par

$$\tau = \mathbf{M}(\theta)\ddot{\theta} + \mathbf{h}(\theta, \dot{\theta}) + \mathbf{V}\dot{\theta} + \mathbf{g}(\theta) \quad (3.1)$$

où  $\tau$  est le vecteur des couples articulaires,  $\mathbf{M}(\theta)$  est la matrice d'inertie généralisée,  $\theta$  est

le vecteur des coordonnées articulaires,  $\mathbf{h}(\boldsymbol{\theta}, \dot{\boldsymbol{\theta}})$  est le terme relié aux forces de Coriolis et centrifuges,  $\mathbf{V}$  est la matrice des coefficients de frottement des articulations et  $\mathbf{g}(\boldsymbol{\theta})$  est le vecteur des forces dues à la gravité. De plus, puisque les actionneurs sont reliés aux articulations par le biais de réducteurs, on définit

$$\mathbf{G}_r \boldsymbol{\theta} = \boldsymbol{\theta}_a \quad (3.2)$$

où  $\boldsymbol{\theta}_a$  est le vecteur représentant le mouvement des actionneurs et  $\mathbf{G}_r$  est la matrice des rapports de réduction. On modélise également les actionneurs avec l'équation classique suivante :

$$\boldsymbol{\tau}_m = \mathbf{M}_a \ddot{\boldsymbol{\theta}}_a + \mathbf{V}_a \dot{\boldsymbol{\theta}}_a + \boldsymbol{\tau}_a \quad (3.3)$$

où  $\mathbf{M}_a$  est une matrice diagonale dont l'élément  $ii$  est l'inertie du  $i^e$  actionneur,  $\mathbf{V}_a$  est la matrice diagonale des coefficients de frottement des actionneurs,  $\boldsymbol{\tau}_a$  est le vecteur des couples transmis aux réducteurs reliés aux articulations et  $\boldsymbol{\tau}_m$  est le couple résultant aux actionneurs.

La relation (3.2) et le principe du travail virtuel permettent aussi d'écrire

$$\boldsymbol{\tau} = \mathbf{G}_r^T \boldsymbol{\tau}_a. \quad (3.4)$$

En combinant les équations (3.1) à (3.4), on obtient le modèle dynamique du système complet :

$$\mathbf{G}_r^T \boldsymbol{\tau}_m = [\mathbf{G}_r^T \mathbf{M}_a \mathbf{G}_r + \mathbf{M}(\boldsymbol{\theta})] \ddot{\boldsymbol{\theta}} + \mathbf{h}(\boldsymbol{\theta}, \dot{\boldsymbol{\theta}}) + [\mathbf{G}_r^T \mathbf{V}_a \mathbf{G}_r + \mathbf{V}] \dot{\boldsymbol{\theta}} + \mathbf{g}(\boldsymbol{\theta}) \quad (3.5)$$

avec les matrices  $\mathbf{M}_a$ ,  $\mathbf{V}_a$  et  $\mathbf{G}_r$  qui sont diagonales si chaque actionneur n'est relié qu'à une seule articulation.

Par conséquent, suivant l'équation (3.5), une hypothèse valide lorsque le rapport de réduction d'un moteur est suffisamment élevé est de considérer que le couple nécessaire pour accélérer le rotor du moteur est dominant par rapport aux autres couples. Les autres couples, tels que ceux reliés aux forces de Coriolis, ou ceux qui résultent de l'inertie des membrures, peuvent donc être négligés. Enfin, pour le cas considéré dans ce mémoire, le vecteur de couples dus à la gravité n'est pas considéré, étant donné que le robot est en chute libre.

Il est bien entendu délicat de déterminer le seuil à partir duquel cette hypothèse est valide. En l'occurrence, cette hypothèse a été utilisée en considérant le rapport de réduction relativement élevé des moteurs (24 :1) et en supposant que la loi de commande PID en parallèle allait corriger les erreurs de modélisation qui en découleraient. Au final, l'expérience a démontré que cette stratégie de commande était suffisamment performante à toutes fins pratiques.

### 3.2.3 Méthodes de mesure

Tel que mentionné aux chapitres précédents, les premières mesures expérimentales ont été prises avec une caméra haute-vitesse. Bien que ces données donnent une meilleure vue d'ensemble et de l'information plus riche sur la manœuvre de réorientation, elles demeurent entièrement qualitatives. Il est donc extrêmement ardu, voire impossible, d'extraire des informations quantitatives de ces données dans l'optique de les comparer à un modèle théorique.

Par conséquent, la solution retenue pour récolter des données quantitatives a été l'utilisation d'un système de capture de mouvements, plus précisément celui de la compagnie Vicon. Ce système fonctionne à l'aide d'un ensemble de caméras infra-rouges qui suivent des marqueurs passifs réfléchissants. Les marqueurs, de forme sphérique, apparaissent sous forme de cercles dans le plan image de chaque caméra et leur centre peut ainsi être trouvé aisément. En sachant la position et l'orientation de chaque caméra, le système peut projeter virtuellement dans l'espace un rayon passant par le centre des marqueurs dans le plan image. La position des marqueurs dans l'espace est déterminée à partir des points d'intersection des rayons projetés. Il faut donc que les marqueurs soient visibles par plusieurs caméras simultanément.

Le montage utilisé pour la prise de données inclut huit caméras disposées sur le périmètre d'une salle, au centre de laquelle est placé le poteau de lancement présenté à la section 3.2.1. Pour suivre un corps rigide dans l'espace, le système Vicon a besoin d'au moins trois marqueurs visibles en tout temps. L'ajout de marqueurs supplémentaires sur le corps permet une redondance d'information et augmente la fiabilité, en particulier lorsqu'un marqueur est momentanément caché. En l'occurrence, cinq marqueurs ont été disposés sur la première membrure du robot pour respecter les contraintes d'espace, tel que montré à la Figure 2.11. Ceux-ci ont aussi dû être disposés de façon à ne pas nuire aux mouvements pendant les manœuvres de réorientation. Seule la première membrure du robot est suivie, afin de simplifier la prise de mesure et d'éviter la mauvaise attribution des marqueurs entre les corps par le logiciel de traitement. Par ailleurs, l'information sur les autres corps n'est pas nécessaire, puisque l'architecture du robot est de type serielle. Par conséquent, connaissant la position et l'orientation de la première membrure et la position angulaire de chaque articulation, la position et l'orientation de chacune des membrures peuvent facilement être calculées.

Pour que le système Vicon puisse suivre un ou plusieurs corps rigides plutôt que chaque marqueur individuel, il faut définir un modèle dans le logiciel. La définition du modèle se fait en spécifiant les marqueurs qui appartiennent au même corps. Ensuite, lors de la prise de données, le système de traitement tente d'ajuster le modèle aux données expérimentales obtenues.

### 3.2.4 Comparaison des données

La comparaison entre les données expérimentales et celles issues de la simulation numérique constitue un problème typique de changement de repère. En effet, les systèmes d'axes dans la simulation n'ont pas nécessairement les mêmes orientations que dans le logiciel de traitement du système Vicon. Ainsi, pour comparer les résultats, il faut d'abord rapporter toutes les données dans le même repère de coordonnées. La Figure 3.6 présente le schéma du problème.

Dans cette figure, le repère  $V$  correspond au repère de base du système Vicon et le repère  $N$  correspond au repère de base dans Siemens NX. Les repères  $R_V$  et  $R_N$  représentent quant

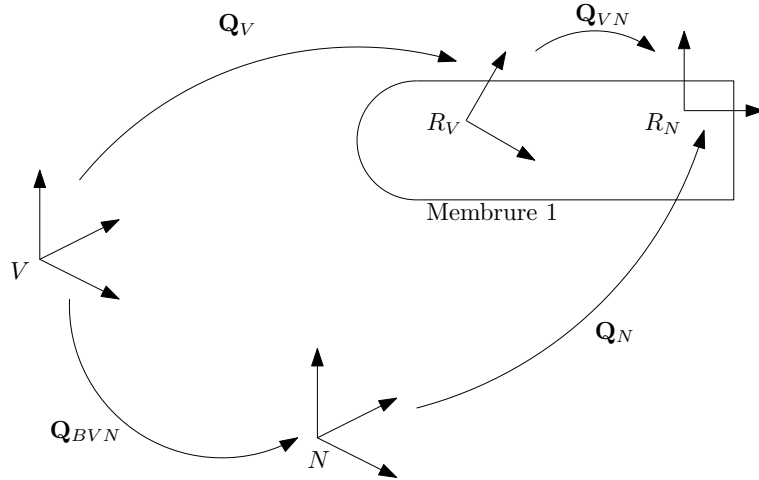


FIGURE 3.6 – Schéma du problème de changements de repère

à eux le système d'axe associé au modèle de la première membrure dans le système Vicon et dans Siemens NX, respectivement. La transformation  $\mathbf{Q}_V$  est la mesure de l'orientation du modèle par rapport à l'origine du système Vicon, c'est-à-dire la rotation de  $V$  vers  $R_V$ , alors que  $\mathbf{Q}_N$  donne l'orientation du modèle par rapport à l'origine de Siemens NX.  $\mathbf{Q}_{BVN}$  représente la rotation du repère de base  $V$  au repère de base  $N$  et  $\mathbf{Q}_{VN}$  représente la rotation de  $R_V$  vers  $R_N$ . Puisque l'on ne s'intéresse qu'aux données d'orientation et non de position, seules les rotations entre les repères sont considérées et les translations sont ignorées.

Afin de comparer les mesures expérimentales aux résultats de la simulation, on cherche donc à exprimer  $\mathbf{Q}_N$  en fonction de  $\mathbf{Q}_V$ . En d'autres mots, on rapporte les mesures expérimentales  $\mathbf{Q}_V$  fournies par le système Vicon dans le repère de base  $N$  de Siemens NX. Sous forme d'équation, en se basant sur le schéma à la Figure 3.6, on obtient :

$$\mathbf{Q}_N = \mathbf{Q}_{BVN}^T \mathbf{Q}_V \mathbf{Q}_{VN}. \quad (3.6)$$

Puisque le repère de base  $V$  est défini manuellement lors de la calibration du système Vicon,  $\mathbf{Q}_{BVN}$  est connue. Il reste toutefois une inconnue, qui est la matrice de rotation  $\mathbf{Q}_{VN}$ . En effet, bien que le repère  $R_N$ , provenant d'un logiciel de CAO, puisse être considéré comme étant aligné sur la géométrie de la membrure (les axes sont parallèles aux arêtes géométriques) on ne peut en dire autant du repère  $R_V$ . Ce dernier est orienté par défaut selon le positionnement des marqueurs et leur ordre de sélection dans le logiciel Vicon. Par ailleurs, le positionnement des marqueurs est souvent approximatif et ne permet pas toujours d'aligner le système d'axes sur des éléments géométriques. Pour remédier à ce problème, une solution développée au Laboratoire de vision et systèmes numériques de l'Université Laval consiste à utiliser une pointe à tracer à laquelle est attachée un marqueur réfléchissant. Cet outil permet de pointer des éléments physiques alors que le système Vicon fait des lectures, dans le but de modifier l'orientation du système d'axes du modèle. En alignant ainsi le système d'axes  $R_V$  sur la

géométrie de la membrure, on peut, par exemple, imposer que la rotation  $\mathbf{Q}_{VN}$  soit l'identité, ou encore une succession de rotations simples à exprimer analytiquement.

Finalement, le système Vicon fournit indirectement la matrice  $\mathbf{Q}_V$  avec une représentation par angles d'Euler suivant une convention XYZ. Par conséquent, on obtient

$$\mathbf{Q}_V = \mathbf{Q}_X(\alpha)\mathbf{Q}_Y(\beta)\mathbf{Q}_Z(\gamma) \quad (3.7)$$

où  $\alpha$ ,  $\beta$ , et  $\gamma$  sont les 3 angles d'Euler selon les axes  $X$ ,  $Y$  et  $Z$  respectivement et où

$$\mathbf{Q}_X(\alpha) = \begin{bmatrix} 1 & 0 & 0 \\ 0 & \cos(\alpha) & -\sin(\alpha) \\ 0 & \sin(\alpha) & \cos(\alpha) \end{bmatrix} \quad (3.8)$$

$$\mathbf{Q}_Y(\beta) = \begin{bmatrix} \cos(\beta) & 0 & \sin(\beta) \\ 0 & 1 & 0 \\ -\sin(\beta) & 0 & \cos(\beta) \end{bmatrix} \quad (3.9)$$

$$\mathbf{Q}_Z(\gamma) = \begin{bmatrix} \cos(\gamma) & -\sin(\gamma) & 0 \\ \sin(\gamma) & \cos(\gamma) & 0 \\ 0 & 0 & 1 \end{bmatrix}. \quad (3.10)$$

Une fois la matrice de rotation  $\mathbf{Q}_V$  calculée, celle-ci est décomposée en angles d'Euler en suivant la convention utilisée par Siemens NX, afin de pouvoir présenter une comparaison graphique des courbes.

### 3.3 Conclusion

Ce chapitre a présenté la méthodologie utilisée pour les travaux de simulation et la validation expérimentale des résultats. Le processus de simulation fait appel à un modèle provenant de Siemens NX imbriqué dans un script MATLAB pour étudier des paramètres de façon itérative. Pour la validation expérimentale, le principe de tour d'apesanteur a été utilisé et le robot a été commandé par un système temps réel basé sur la plateforme RT-Lab. Le schéma de commande du robot implique un contrôleur PID aidé d'information sur les couples pré-calculés. Les données quantitatives sur l'orientation du robot sont obtenues par le biais d'un système de capture de mouvements Vicon, puis des calculs de changements de repère permettent leur comparaison avec les résultats des simulations.

### 3.4 Bibliographie

A. J. Koivo. *Fundamentals for control of robotic manipulators*. Wiley, 1989.

# Conclusion

Ce mémoire a abordé la problématique de la réorientation de robots articulés en chute libre ou en apesanteur avec un moment cinétique nul. L'objectif était de développer une méthode permettant des rotations nettes par le biais de mouvements internes, sous la contrainte que le robot doive ultimement retourner à sa configuration initiale dans l'espace articulaire. De plus, le robot devait respecter des limites articulaires afin d'éviter d'entrer en collision avec lui-même.

Le premier chapitre a introduit une première manoeuvre permettant au robot d'exécuter une rotation nette d'environ 180 degrés suivant son axe longitudinal. Cette séquence de mouvements, semblable au réflexe de redressement du chat, a d'abord été étudiée en simulation pour identifier les paramètres d'influence. Les résultats de la simulation ont notamment montré que le comportement de la réorientation est stable : une plus grande amplitude de déplacements articulaires résulte en une plus grande rotation nette. La simulation a aussi permis d'identifier des valeurs pour certaines propriétés dynamiques ayant un effet favorable sur la réorientation. Ces résultats ont finalement été validés expérimentalement à l'aide d'un prototype robotique, de séquences vidéo haute vitesse et d'un système de capture de mouvements.

Le second chapitre a repris les résultats initiaux pour approfondir l'analyse et proposer une deuxième manoeuvre de réorientation. Cette dernière a également été évaluée en simulation, avec comme conclusion que son comportement est prévisible, malgré qu'elle ne permette qu'une amplitude de rotation moindre. Ensuite, il a été démontré, en s'appuyant sur la littérature existante, qu'en combinant cette manoeuvre supplémentaire avec la première, n'importe quelle orientation dans l'espace est atteignable. À titre d'exemple, par le biais d'une simulation, il a été montré qu'une séquence spécifique de manoeuvres donnait lieu à une rotation nette qui est impossible à réaliser si l'on utilise uniquement la première ou la deuxième manoeuvre.

Le troisième chapitre a présenté de façon détaillée la méthodologie qui a mené à l'obtention des résultats. Ainsi, un modèle élaboré dans un logiciel commercial de simulation dynamique, intégré à un programme MATLAB, a généré les résultats préliminaires. Ces résultats ont notamment servi à valider la faisabilité des trajectoires de réorientation en fonction de l'équipement disponible. Les données de simulation ont aussi été mises à profit afin d'améliorer la commande du robot. Enfin, la stratégie de mesure, utilisant un système VICON, de même que

la méthode de changement de repères permettant d'interpréter ces données, ont été explicitées.

À travers l'atteinte de l'objectif de recherche, ces travaux ont résulté en plusieurs apports. Notamment, les manoeuvres proposées permettent la réorientation de robots ayant une architecture plus complexe. En effet, les manoeuvres peuvent s'appliquer aux manipulateurs classiques à sept degrés de liberté, sans nécessiter de composantes additionnelles telles que des roues d'inertie ou des joints de Cardan. Par ailleurs, ces manoeuvres sont réalistes au sens où elles prennent en considération les limites articulaires du robot. Enfin, l'un des principaux intérêts est que tout cela soit rendu possible en trois dimensions et que les réorientations ne soient donc pas cloisonnées à l'espace plan.

Pour conclure, il reste malgré tout un important travail à accomplir. En l'occurrence, bien que les manoeuvres présentées rendent possible une réorientation arbitraire, il serait très intéressant de développer une méthode qui permettrait la synthèse automatique de séquences de manoeuvres. Une telle méthode pourrait par ailleurs considérer puis corriger les perturbations dans l'orientation du robot, afin d'obtenir au final un processus en boucle fermée.

# Bibliographie

- J.-A. Bettez-Bouchard and C. Gosselin. Development and experimental validation of a re-orientation algorithm for a free-floating serial manipulator. In *2016 IEEE International Conference on Robotics and Automation (ICRA)*, pages 2733–2738. IEEE, may 2016.
- J. T. Bingham, J. Lee, R. N. Haksar, J. Ueda, and C. K. Liu. Orienting in mid-air through configuration changes to achieve a rolling landing for reducing impact after a fall. In *2014 IEEE/RSJ International Conference on Intelligent Robots and Systems*, pages 3610–3617. IEEE, sep 2014.
- E. Chang-Siu, T. Libby, M. Tomizuka, and R. J. Full. A lizard-inspired active tail enables rapid maneuvers and dynamic stabilization in a terrestrial robot. In *2011 IEEE/RSJ International Conference on Intelligent Robots and Systems*, pages 1887–1894. IEEE, sep 2011.
- E. Chang-Siu, T. Libby, M. Brown, R. J. Full, and M. Tomizuka. A nonlinear feedback controller for aerial self-righting by a tailed robot. In *2013 IEEE International Conference on Robotics and Automation*, pages 32–39. IEEE, may 2013.
- D. D'Alessandro. Optimal evaluation of generalized Euler angles with applications to control. *Automatica*, 40(11) :1997–2002, nov 2004.
- S. Dubowsky and E. Papadopoulos. The kinematics, dynamics, and control of free-flying and free-floating space robotic systems. *IEEE Transactions on Robotics and Automation*, 9(5) :531–543, 1993.
- A. Flores-Abad, O. Ma, K. Pham, and S. Ulrich. A review of space robotics technologies for on-orbit servicing. *Progress in Aerospace Sciences*, 68 :1–26, jul 2014.
- C. Frohlich. Do springboard divers violate angular momentum conservation? *American Journal of Physics*, 47(7) :583–592, jul 1979.
- C. Frohlich. The Physics of Somersaulting and Twisting. *Scientific American*, 242 :154–165, 1980.
- M. Hamada. The minimum number of rotations about two axes for constructing an arbitrarily fixed rotation. *Royal Society open science*, 1(3) :140145, nov 2014.

- A. Jusufi, D. T. Kawano, T. Libby, and R. J. Full. Righting and turning in mid-air using appendage inertia : Reptile tails, analytical models and bio-inspired robots. *Bioinspir. Biomim.* 5 045001 *Bioinsp. Biomim.*, 5 :45001–12, 2010.
- T. Kane and M. Scher. Human self-rotation by means of limb movements. *Journal of Biomechanics*, 3(1) :39–49, jan 1970.
- T. R. Kane and M. P. Scher. A dynamical explanation of the falling cat phenomenon. *International Journal of Solids and Structures*, 5(7) :663–670, 1969.
- T. Kawamura. Understanding of Falling Cat Phenomenon and Realization by Robot. *Journal of Robotics and Mechatronics*, 26(6) :685–690, dec 2014.
- A. J. Koivo. *Fundamentals for control of robotic manipulators*. Wiley, 1989.
- I. Kolmanovsky, N. H. McClamroch, and V. T. Coppola. New results on control of multibody systems which conserve angular momentum. *Journal of Dynamical and Control Systems*, 1 (4) :447–462, oct 1995.
- P. V. Kulwicki, E. J. Schlei, and P. L. Vergamini. Weightless man : Self-rotation techniques. Technical report, Air Force Aerospace Medical Research Lab, 1962.
- T. Libby, A. M. Johnson, E. Chang-Siu, R. J. Full, and D. E. Koditschek. Comparative Design, Scaling, and Control of Appendages for Inertial Reorientation. *IEEE Transactions on Robotics*, 32(6) :1380–1398, dec 2016.
- F. Lowenthal. Uniform finite generation of the rotation group. *Rocky Mountain Journal of Mathematics*, 1(4) :575–586, dec 1971.
- T. W. Mather and M. Yim. Modular configuration design for a controlled fall. In *2009 IEEE/RSJ International Conference on Intelligent Robots and Systems*, pages 5905–5910. IEEE, oct 2009.
- M. Reyhanoglu and N. H. McClamroch. Planar reorientation maneuvers of space multibody systems using internal controls. *Journal of Guidance, Control, and Dynamics*, 15(6) :1475–1480, nov 1992.
- C. Rui, I. Kolmanovsky, and N. McClamroch. Control problems for a multibody spacecraft via shape changes : constant nonzero angular momentum. In *Proceedings of the 1997 American Control Conference (Cat. No.97CH36041)*, pages 1904–1908 vol.3. IEEE, 1997.
- C. Rui, I. Kolmanovsky, and N. McClamroch. Nonlinear attitude and shape control of spacecraft with articulated appendages and reaction wheels. *IEEE Transactions on Automatic Control*, 45(8) :1455–1469, 2000.

- A. Shapere and F. Wilczek. Gauge kinematics of deformable bodies. *American Journal of Physics*, 57(6) :514–518, jun 1989.
- A. D. Shapere. *Gauge mechanics of deformable bodies*. PhD thesis, University of California, Santa Barbara, 1988.
- P. G. Smith and T. R. Kane. The Reorientation of a Human Being in Free Fall. 1967.
- L. A. Stirling. Development of astronaut reorientation methods : a computational and experimental study. 2008.
- G. Wenger, A. De, and D. E. Koditschek. Frontal plane stabilization and hopping with a 2DOF tail. In *2016 IEEE/RSJ International Conference on Intelligent Robots and Systems (IROS)*, pages 567–573. IEEE, oct 2016.
- J. Wittenburg. *Dynamics of multibody systems*. Springer Science & Business Media, 2007.
- E. C.-Y. Yang, P. C.-P. Chao, and C.-K. Sung. Optimal Control of an Under-Actuated System for Landing With Desired Postures. *IEEE Transactions on Control Systems Technology*, 19(2) :248–255, mar 2011.
- K. Yoshida and Y. Umetani. Control of Space Manipulators with Generalized Jacobian Matrix. pages 165–204. Springer, Boston, MA, 1993.
- J. Zhao, T. Zhao, N. Xi, M. W. Mutka, and L. Xiao. MSU Tailbot : Controlling Aerial Maneuver of a Miniature-Tailed Jumping Robot. *IEEE/ASME Transactions on Mechatronics*, 20(6) :2903–2914, dec 2015.
- J. Zhao, L. Li, and B. Feng. Effect of swing legs on turning motion of a free-falling cat robot. In *2017 IEEE International Conference on Mechatronics and Automation (ICMA)*, pages 658–664. IEEE, aug 2017.